



OPEN Dynamic monitoring of ecological security patterns in arid zone oases: a remote sensing-based ecological index evolution analysis

Longlong Zhang, Jiaqi Zhai✉, Fan He, Xing Li & Tao Wang

As vital biological hubs in delicate ecosystems, oasis in arid zones provide vital ecosystem services that include resource availability, biodiversity preservation, and temperature management. The quantitative contributions of human and climatic causes to the dynamics of eco-environmental quality are still not well understood, despite their importance. This study evaluates the evolution of EEQ in three dry irrigation oasis in China (Hetao, Ningxia, and Minqin) between 2000 and 2022 by utilizing Google Earth Engine to create a Remote Sensing Ecological Index that integrates multi-dimensional indicators. We determine that precipitation is the primary driver using Shapley additive explanations (SHAP) in conjunction with interpretable machine learning; the corresponding SHAP values are 0.031, 0.063, and 0.30. Critical thresholds that signaled a change from ecosystem suppression to enhancement appeared at 164 mm/yr for PRE and 1218 mm/yr for irrigation volume (IV). In terms of geography, 99% of RSEI values were in the medium-to-poor range, exhibiting varying patterns: stability in Minqin, improvement in Ningxia, and slight decline in Hetao. RSEI is positively impacted by ecological water replenishment, but urbanization and grassland degradation have negative impacts. A decision framework for ecological restoration project optimization is established by these threshold-driven insights, which are especially pertinent to attaining land degradation neutrality in drylands across the world.

Keywords Arid irrigation oases, Shapley additive explanations, Interpretable machine learning, RSEI, EEQ

Natural ecological settings are integrally related to human life, productivity, and survival¹. Their quality constitutes a vital indicator for evaluating the coordination between regional socioeconomic development and natural environments². According to the IPCC's "2006 IPCC Guidelines for National Greenhouse Gas Inventories (2019 Refinement)" (IPCC, 2019), recent increases in global warming and human activity have had a significant influence on ecological-environmental systems in many different places. These factors have caused a number of ecological and environmental problems, drastically changed the quality of the regional eco-environment, and increasingly jeopardized the ecological security of the region^{3,4}.

Alongside strong economic growth and a rapidly expanding population, environmental degradation has increasingly gained international recognition as a problem of concern. Approximately 41% of the world's geographical surface is made up of arid and semi-arid areas, which are among the most fragile ecosystems on Earth. These regions exhibit increased susceptibility to human activity and global warming^{5,6}. The extension of arid/semi-arid zones and the escalation of hydrological cycles have worsened ecological degradation in the context of global environmental degradation, consequently posing serious concerns to sustainable socioeconomic development globally⁷. Therefore, conducting real-time ecological state assessments, formulating scientific conservation strategies, and promoting high-quality socioeconomic development all heavily rely on the quantitative monitoring of EEQ and the precise understanding of its evolutionary patterns.

With the continuous advancement of satellite remote sensing technology and Geographic Information Systems (GIS) technologies, the monitoring and assessment of eco-environmental quality in arid and semi-arid regions has been enabled with accurate and efficient technical support. For the assessment of EEQ, early research mostly used single remote sensing indicators, such as the land surface temperature (LST), leaf area index (LAI)⁸, and normalized difference vegetation index (NDVI)⁹. However, scholars generally consider ecosystems to be complex systems, in which a single indicator cannot fully capture the status of regional ecological environments.

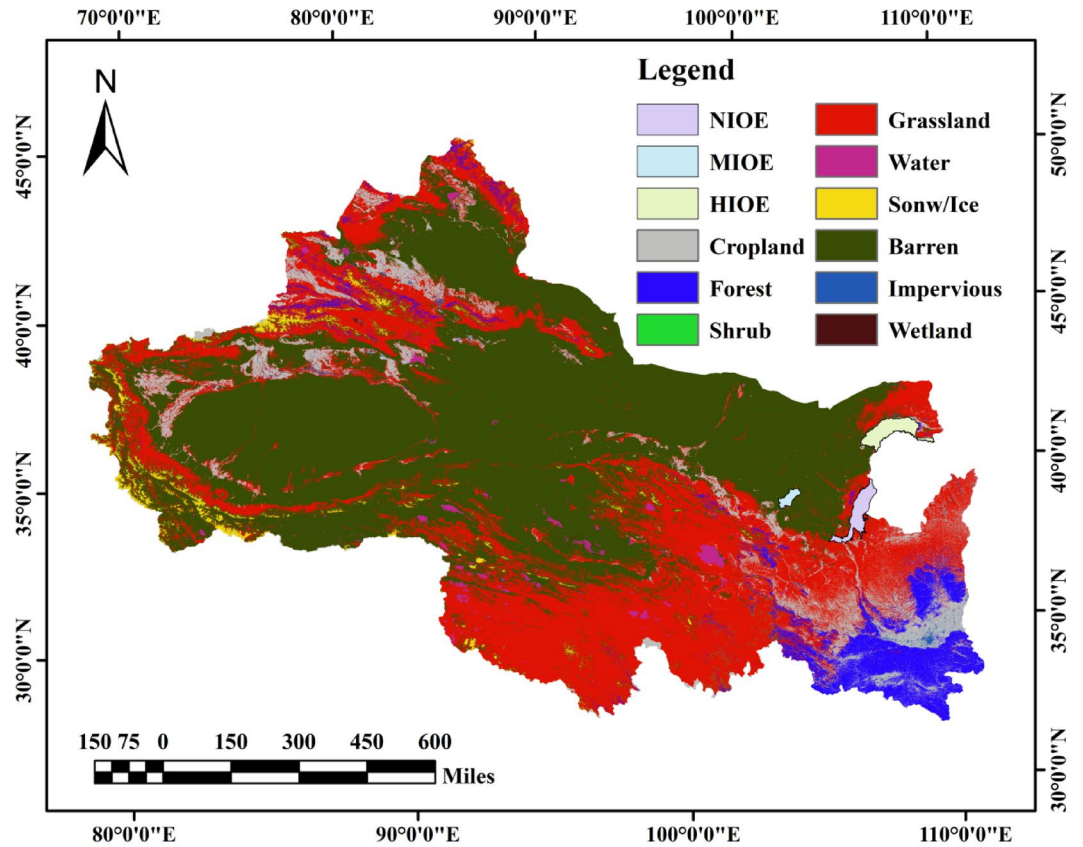
State Key Laboratory of Water Cycle and Water Security, China Institute of Water Resources and Hydropower Research, Beijing 100038, China. ✉email: jiaqizhai@163.com

The Press-State-Response (PSR) model was jointly suggested by the Organization for Economic Co-operation and Development (OECD) and the United Nations Environment Programme (UNEP)¹⁰. Other scholars have also proposed models such as the ecological footprint model¹¹, ecological resilience assessment¹², and environmental index (EI)¹³, establishing fundamental methodological frameworks for eco-environmental quality evaluation. To create assessment systems like ecological vulnerability assessment models, several researchers have included various ecological environment indicators (such as socioeconomic aspects and ground observations)¹⁴. Xu developed the Remote Sensing Ecological Index (RSEI) by integrating four core components—NDVI, wetness (WET), LST, and NDBSI. These components are highly consistent with the core ecological elements of “vegetation–moisture” in oases and possess distinctive advantages in characterizing the eco-environmental quality of oasis systems¹⁵. Understanding ecological status and its temporal dynamics is made possible by this index, which uses principal component analysis for weight assignment to provide a quantitative, quick, and impartial assessment of urban and regional ecological habitats. At different geographic scales, this method is now frequently employed in EEQ research^{16,17}. In order to establish theoretical and scientific underpinnings for regional ecological conservation, Li Shangzhi et al. examined ecological changes in the Hetao Yellow River Irrigation Oasis using a variety of environmental parameters and RSEI¹⁸. They also looked at anthropogenic influences on ecosystems. In order to overcome the inadequacy and instability of the RSEI, Wang Ziwei et al. developed a unique road surface ecological simulation index based on the conventional RSEI, which can be applied to monitor water-rich urban environments and demonstrates stability and multifunctionality across cities with different ecological contexts¹⁹. The selection of diverse indicators in the RSEI framework, which involves heterogeneous datasets and complex computational models, often results in large data volumes and intricate processing workflows. These challenges constrain its applicability for long-term, large-scale monitoring of EEQ in arid and semi-arid regions. Leveraging its capacity to access and process massive time-series remote sensing datasets, the GEE platform provides an effective solution to overcome these limitations.

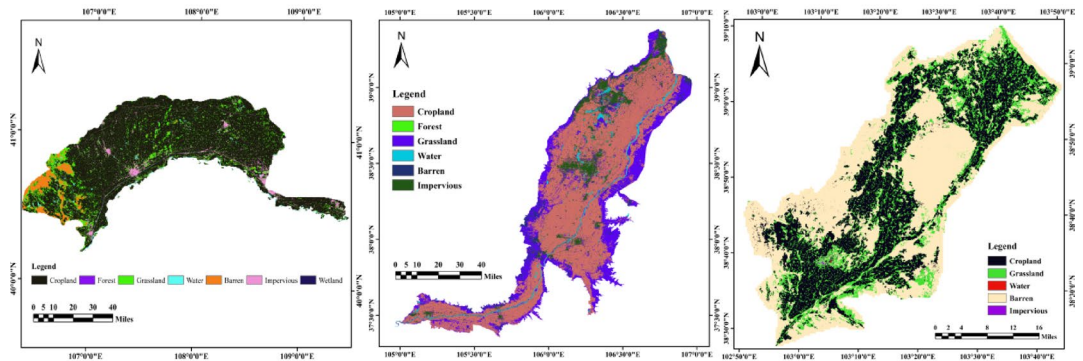
In arid and semi-arid oasis ecosystems, EEQ is influenced by both natural and anthropogenic drivers, including climate change, topography, land cover, and socio-economic conditions^{20,21}. Traditional statistical methods (e.g., regression and correlation analysis) rely on assumptions of spatial independence and linearity, making them unsuitable for capturing nonlinear interactions among multiple factors. Geographic detectors and geographically weighted regression (GWR) offer advances in identifying spatial heterogeneity and local effects, but remain constrained by limitations in effect direction and covariate collinearity²². Recent advances in machine learning provide powerful tools for modeling nonlinear and high-dimensional relationships, yet their “black-box” nature reduces transparency and hinders decision-making. By incorporating SHAP, Zhang et al. improved the interpretability and reliability of machine learning models, enabling better understanding of factor contributions, enhancing predictive credibility, and offering new insights into EEQ dynamics²³.

Hetao Irrigated Oasis Ecosystem (HIOE) (106°20′–109°19′E, 40°19′–41°18′N)¹⁸, Ningxia Irrigated Oasis Ecosystem (NIOE) (104°19′–106°56′E, 37°23′–39°23′N), and Minqin Irrigated Oasis Ecosystem (MIOE) (102°03′–104°03′E, 38°05′–39°06′N) are three representative irrigated oases in arid regions of northwestern China, with a total study area of 25,000 km² (Fig. 1). The region is characterized by a temperate continental climate with high evapotranspiration, sparse vegetation, and fragile ecosystems, where annual precipitation is generally below 200 mm and water supply largely depends on external diversion. Since the 1970s, large-scale ecological restoration and water-saving irrigation projects have been implemented, including the Beijing-Tianjin Sand Source Control Project (DCBT) and the expansion of 4467 km² of efficient irrigation during the 13th Five-Year Plan. This engineering measure enhances vegetation cover by increasing water supply and mitigating land desertification, thereby improving ecosystem stability and productivity. Simultaneously, it effectively restrains sandification and soil salinization processes, resulting in an overall improvement of regional EEQ. Nevertheless, the ecosystems remain vulnerable, facing risks of declining greenness and degradation. In some areas, the synergy between ecological restoration and water resource management has been overlooked^[24–26]. Vegetation cover has approached the regional carrying capacity, where enhanced transpiration intensifies the water cycle, and irrigation-driven soil water recharge further aggravates salinization, thereby accelerating vegetation decline. This raises a key scientific question: under the combined impacts of climate change and human activities, what are the trajectories and driving mechanisms of EEQ in irrigated oases of arid and semi-arid regions? To ensure sustainable ecological improvements, it is essential to accurately assess EEQ dynamics and disentangle the interactions among driving factors. However, most existing studies rely on single indicators or localized assessments of combined indices, without explicitly distinguishing between positive and negative drivers. Comprehensive assessments of EEQ and the bidirectional interactions of its determinants across irrigated oases in arid regions remain scarce. The framework of this study is illustrated in Fig. 2.

In order to determine the RSEI as a stand-in for EEQ in dry zone oases, this study used MODIS data from the GEE cloud computing platform. Current and prospective EEQ trajectories were revealed using the Hurst index, Mann–Kendall test, and Theil–Sen median trend analysis. Disentangling driving elements was done using an interpretable machine learning model. The study aims to: determine the key causes of EEQ variances at the regional and sub-zonal levels, elucidating the functions of irrigation with water diversion and climate conditions; identify the critical factor thresholds that either support or impede the improvement of EEQ at both the holistic and divided spatial scales; and examine the spatiotemporal dynamics of EEQ in desert oasis for the last 23 years, evaluate how well it aligns with changes in plant greening, and compile regional differences and spatial patterns. The results give theoretical references for tackling ecological issues in oases in dry zones, improve regional ecosystem resilience under climate change, and inform focused ecological restoration methods.



a



b

c

d

Fig. 1. Overview map of the study area (a. Northwest China; b. HIOE; c. NIOE; d. MIOE.) (version QGIS 3.28; <https://qgis.org/en/site/forusers/download.html>).

Methods

Data preprocessing

The 500 m surface reflectance (MOD09A1), 1 km land surface temperature (MOD11A2 V6), and 500 m NDVI (MOD13A1 V6) MODIS datasets (2000–2022) were used in this investigation on the GEE. Preprocessing of the data included normalization within the research region, spatial harmonization to 1 km resolution using bilinear interpolation, and cloud/water masking. Eight EEQ drivers—PRI, potential evapotranspiration (PET)²⁷, soil moisture content (SMC)²⁸, fractional vegetation cover (FVC)²⁹, land use change (LUCC)³⁰, IV³¹, nighttime light (NL)³², and population density (POP)³³—were assessed using an analysis of 421,330 grids (1×1 km), excluding water bodies in compliance with RSEI methodology (Table 1). The methodology measured the EEQ dynamics

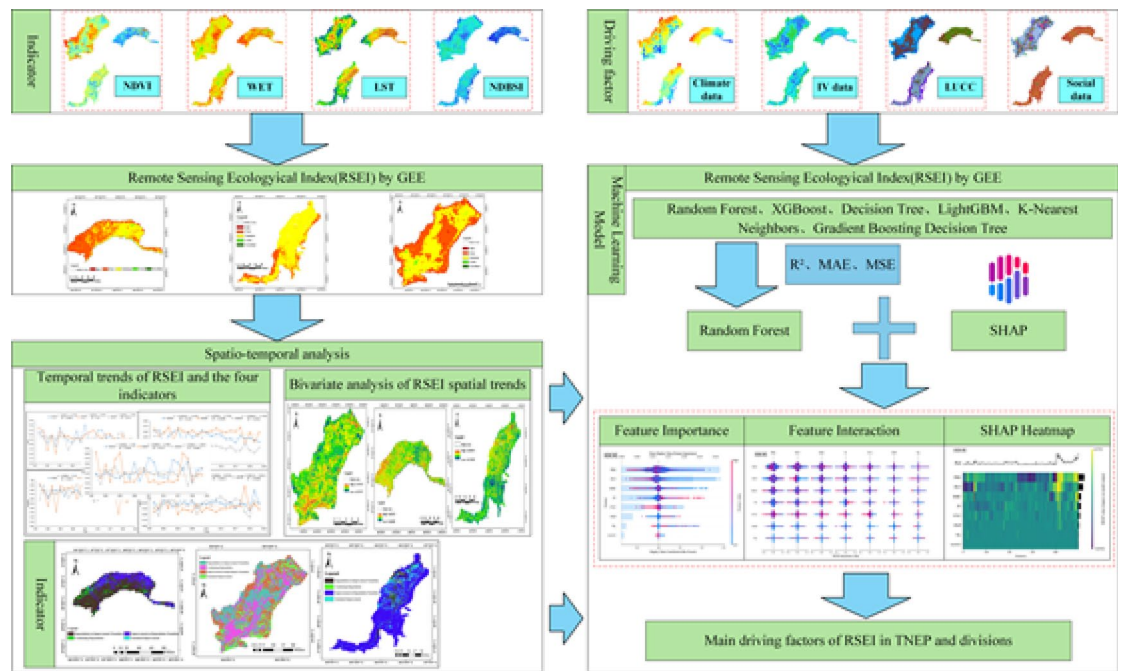


Fig. 2. Framework of the study.

Data type	Data name	Description	Resolution time span	Source
RSEI	MOD09A1	Surface reflectance synthesized products for calculating WET and NDBSI	500 m, 2000–2022	GEE (https://developers.google.com)
	MOD11A2 V6	LST synthesized products	500 m, 2000–2022	
	MOD13A1 V6	NDVI products	500 m, 2000–2022	
Natural factors	Potential evapotranspiration (PET)	Monthly potential evapotranspiration for China	1 km, 2000–2022	National earth system science data center (https://www.geodata.cn)
	Cumulative precipitation (PRE) (mm)	Monthly precipitation for China	1 km, 2000–2022	
	Soil moisture content (SMC)	Yearly soil moisture content for China	500 m, 2000–2022	
	Fractional vegetation cover (FVC)	Yearly fractional vegetation coverage for China	250 m, 2000–2022	
Anthropogenic factors	Land use uncover change (LUCC)	Annual China Land Cover Dataset, CLCD, from Wuhan University	30 m, 2000–2022	https://doi.org/10.5281/zenodo.4417809
	Nighttime-light (NL)	Global “NPP-VIRS-like” nighttime light dataset	500 m, 2000–2022	National earth system science data center, national science & technology infrastructure of China (http://www.geodata.cn)
	Population density (POP)	Landscan Population Density	1 km, 2000–2022	Oak ridge national laboratory https://landscan.ornl.gov/
	Irrigation volume (IV)	Calculation of Grid Irrigation Water Requirements Using WACM	500 m, 2000–2022	Bureau of hydrology

Table 1. Description and sources of data.

of dry oasis across three irrigation systems in northwest China by combining climatic (CMFD), ecological (MODIS), and socioeconomic factors.

RSEI model

By combining four indicators—NDVI, WET, LST, and NDBSI—and using Principal Component Analysis (PCA), the RSEI model thoroughly evaluates eco-environmental quality³⁴.

$$RSEI = f(NDVI, WET, LST, NDBSI)$$

Higher values on the RSEI scale, which goes from 0 to 1, denote better ecological quality. The main component of RSEI, NDVI, is obtained from the MOD13A1 Vegetation Index (VI) dataset. Wetness, which indicates the

moisture content of the surface soil and plants, is calculated using the Tasseled Cap Transformation of MOD09A1 data in the manner described below³⁵:

$$WET = 0.1147\rho_1 + 0.2489\rho_2 + 0.2408\rho_3 + 0.3132\rho_4 - 0.3122\rho_5 - 0.6416\rho_6 - 0.5087\rho_7$$

where $\rho_1 \sim \rho_7$ correspond to the surface reflectance of MOD09A1 bands: Red band, NIR1 band, Blue band, Green band, NIR2 band, SWIR1 band, SWIR2 band.

$$LST = DN \times 0.02 - 273.15$$

where DN denotes the digital number of the LST band.

NDBSI integrates the Soil Index and Index of Bare Soil³⁶, formulated as:

$$NDBSI = (SI + IBI)/2$$

$$IBI = \frac{2SWIR1/(SWIR1 + NIR) - [NIR/(NIR + RED) + GREEN/(GREEN + SWIR1)]}{2SWIR1/(SWIR1 + NIR) - [NIR/(NIR + REN) + GREEN/(GREEN + SWIR1)]}$$

$$SI = \frac{(SWIR1 + RED) - (NIR + BLUE)}{(SWIR1 + REN) + (NIR + BLUE)}$$

where, RED represents the surface reflectance of the MOD09A1 red band, GREEN the green band, BLUE the blue band, NIR the near-infrared band, and SWIR1 the shortwave infrared band 1.

Given the inconsistent measurement scales of the four indicators, normalization is applied to standardize their ranges within the 0–1 interval. The initial $RSEI_0$ is calculated using PCA³⁷.

$$RSEI_0 = 1 - \{PC1 [f(NDVI, WET, LST, NDBSI)]\}$$

$$RSEI_0 = \frac{(RSEI_0 - RSEI_{0-\min})}{(RSEI_{0-\max} - RSEI_{0-\min})}$$

The starting value is denoted by $RSEI_0$, the first principal component by PC1, and the maximum and minimum values of the initial value are denoted by $RSEI_{0-\max}$ and $RSEI_{0-\min}$, respectively.

RSEI trend analysis

The RSEI change patterns in the oasis between 2000 and 2022 are identified using the Theil-Sen Median Trend analysis. By reducing outlier impacts, this non-parametric approach improves trend identification accuracy and offers robust estimates in comparison to traditional linear regression³⁸. This is how the trend slope is computed:

$$\theta = \text{Median} \left(\frac{x_j - x_i}{j - i} \right), V_{j>i}$$

where x_i and x_j represent the RSEI values for year i and year j , respectively, and the median function effectively suppresses outlier interference. $\theta > 0$ indicates EEQ, while a negative slope denotes degradation.

A popular non-parametric technique for determining trend significance is the Mann-Kendall trend test. This method shows robustness to outliers and doesn't assume that the data is normal. Statistically significant improving trend is identified when the standardized test statistic $|Z| \geq 1.96$ ³⁹. The statistic S is computed as:

$$S = \sum_{i=1}^{n-1} \sum_{j=j+1}^n \text{sgn}(x_j - x_i)$$

$$\text{sgn}(x_j - x_i) = \begin{cases} +1, & x_j - x_i > 0 \\ 0, & x_j - x_i = 0 \\ -1, & x_j - x_i < 0 \end{cases}$$

The standardized test statistic Z :

$$Z = \begin{cases} \frac{R - 1}{\sqrt{\text{Var}(R)}}, & R > 0 \\ 0, & R = 0 \\ \frac{R - 1}{\sqrt{\text{Var}(R)}}, & R < 0 \end{cases}$$

where $\text{Var}(R)$ denotes the variance of R . The significance level is set at $\alpha = 0.05$. A significant variation trend is identified when $|Z| \geq 1.96$. The trend classification criteria (Table 2) were adopted from analogous studies³⁹.

θ	Z	Trend
$\theta < -0.0005$	$ Z \geq 1.96$	Significant degradation
$\theta < -0.0005$	$ Z < 1.96$	Slight degradation
$\theta > 0.0005$	$ Z \geq 1.96$	Significant improvement
$\theta > -0.0005$	$ Z < 1.96$	Slight improvement
$-0.0005 \leq \theta \leq 0.0005$	$ Z < 1.96, Z \geq 1.96$	Unchanged

Table 2. Trend level classification.

The hurst index

The index shows how EEQ tendencies continue to exist. Numerous academic fields, including as ecology, hydrology, and climatology, have made extensive use of this measure⁴⁰.

The Hurst index has the following range of values:

- (1) The RSEI time series shows anti-persistence for $0 \leq H < 0.5$, suggesting that future trends will probably go against the current course and reflect unsustainable ecological processes. As H gets closer to 0, the sustainability of trends steadily declines.
- (2) The RSEI time series shows signs of a non-deterministic walk with independent increments when $H = 0.5$, suggesting that its temporal development lacks enduring memory.
- (3) The RSEI time series shows persistent behavior for $0.5 < H < 1$, suggesting that the observed changes are durable and that future trends will follow the existing trajectory. With clear ecological ramifications across the value range, the sustainability gets stronger as H gets closer to 1.

Combining the Hurst index and RSEI trends enables the quantification of ecological change persistence and prediction of future trajectories: $\theta < 0, H > 0.5$, RSEI is still declining; $\theta < 0, H > 0.5$, RSEI's shift from decline to optimization; $\theta > 0, H > 0.5$, RSEI keeps getting better; $\theta > 0, H < 0.5$, RSEI's shift from optimization to decline.

The machine learning model

This study used the RSEI values of several oasis regions as the dependent variable and eight independent variables, including meteorological, socioeconomic, and land use/cover characteristics, to examine the factors influencing RSEI. Six machine learning regression models—Random Forest (RF)⁴¹, XGBoost (XGB)²³, Decision Tree (DT)⁴², LightGBM (LGB)⁴³, K-Nearest Neighbors (KNN)⁴⁴ and Gradient Boosting Decision Tree (GBDT)⁴⁵—were created especially for dry zone oases. The dataset is divided into 20% for testing and 80% for training for each model. Three accuracy metrics—the Coefficient of Determination (R²), Mean Squared Error (MSE), and Mean Absolute Error (MAE)—are used to assess the effectiveness of the model^{46–49}. The best model is chosen for every region based on these indexes. Ultimately, explainable machine learning techniques were used to evaluate the top-performing models, which shed light on the decision-making process and the impact of various factors on RSEI. This method offers useful information for managing the environment and creating policies.

Explainable machine learning with SHAP model

The goal of the SHAP Model, which has its roots in game theory's Shapley value theory, is to improve the interpretability of complicated machine learning models' predictions. A mathematical technique that objectively breaks down model predictions into contributions from each input variable, the Shapley value equitably distributes cooperative advantages. Shapley values are employed in the RSEI study to assess how land-use, socioeconomic, and climatic factors influence variations in the RSEI. Greater contribution of the component to the outcome of the prediction is indicated by a larger value.

The following is the formula:

$$\varphi_j = \sum_{R \subseteq N \setminus \{j\}} \frac{|R|! (|M| - |R| - 1)!}{|M|!} [f(R \cup \{j\}) - f(R)]$$

where, M represents the set of 8 influencing factors (e.g., PRE, FVC), j denotes a specific covariate at a given location, and R is a subset of factors excluding j. $\varphi_j(f)$ is the SHAP value of covariate j, where $f(R)$ is the model's regression output for the subset R. These values are used by the SHAP framework to describe each factor's contribution. SHAP values are produced for every factor-sample pair by creating an explanation that analyzes the machine learning regression model's outputs. This study calculates SHAP values and looks at the SHAP values of several samples for every component in order to assess the overall impact of multiple variables on the RSEI. The article also describes the relationship between the SHAP values of specific variables and the data values that correspond to them, which helps readers better understand how the machine learning model depends on these elements. The study also shows how each component affects the RSEI and how it interacts with other parameters.

Results

Validity analysis of the RSEI model

In 2000, 2005, 2010, 2015, and 2022, the first main component (PC1) contributed at rates of 57.56%, 49.81%, 64.55%, 84.85%, and 69.46%, respectively (Table 3). In all five analyses, the PC1 average 65% of explained variance, with the PC1 proportion reaching as high as 84.85% specifically in 2015, demonstrating its superiority over the other principal components in reflecting the four ecological indicators. Within PC1, WET exhibited opposing loadings to NDVI, LST, and NDBSI. Significant but conflicting effects on regional ecological quality were highlighted by the fact that LST and WET had the highest absolute loadings. Notably, LST and WET exhibited contrasting ecological effects: Enhanced suppression of ecological degradation by WET corresponded to more substantial ecological stress intensification by LST, and vice versa. NDVI and NDBSI, on the other hand, demonstrated somewhat smaller effects. These findings indicate that NDVI, LST, and NDBSI drive ecological transformations through a remarkably predictive synergistic pattern: elevated LST exacerbates ecological impairments concurrent with declining WET compromising ecosystem stress resilience. This emphasizes how important it is to balance thermal and hydrological elements when determining the dynamics of ecosystems.

The relationships between the RSEI and WET, NDVI, LST, and NDBSI in three irrigation oases—HIOE, NIOE, and MIOE—are examined in this study (Fig. 3). The findings reveal spatially divergent significance levels in the correlations of NDVI, LST, WET, and NDBSI with RSEI across distinct arid-region oases. Among these oases, the statistical significance demonstrated a gradient pattern: MIOE exhibited stronger significance than HIOE, which in turn surpassed that of NIOE. These results confirm that RSEI offers a more thorough and representative evaluation of ecological conditions than any one indicator by itself. The validity of RSEI in representing genuine environmental interactions is demonstrated by the observed correlations, which are consistent with ecological dynamics found in the real world.

Spatial distribution analysis of RSEI

The geographical correlations between the RSEI and the four variables were shown by bivariate analysis (Fig. 4). While LST and NDBSI showed opposing spatial patterns, the NDVI and WET distributions matched the RSEI geographically. Higher surface temperatures and dryness indices, as well as less plant cover, were characteristics

Year	Indicator	PC1	PC2	PC3	PC4
2000	NDVI	-0.12	0.46	0.86	0.20
	LST	-0.74	-0.64	0.23	0.03
	WET	0.61	-0.55	0.46	-0.33
	NDBSI	-0.27	0.27	0.03	-0.92
	Feature value	0.02	0.01	0.00	0.00
	Contribution rate	57.56	26.68	13.50	2.26
2005	NDVI	0.18	0.46	-0.85	0.19
	LST	0.82	-0.55	-0.11	0.06
	WET	-0.39	-0.55	-0.50	-0.55
	NDBSI	0.37	0.43	0.14	-0.81
	Feature value	0.01	0.01	0.00	0.00
	Contribution rate	49.81	33.04	13.93	3.22
2010	NDVI	0.01	0.20	0.97	-0.14
	LST	0.98	-0.17	0.02	-0.02
	WET	-0.14	-0.82	0.25	0.50
	NDBSI	0.11	0.51	0.02	0.85
	Feature value	0.03	0.01	0.00	0.00
	Contribution rate	64.55	21.76	10.95	2.73
2015	NDVI	-0.09	-0.14	-0.98	0.07
	LST	-0.19	-0.96	0.15	-0.12
	WET	0.61	-0.04	-0.11	-0.78
	NDBSI	-0.76	0.22	0.00	-0.61
	Feature value	0.09	0.01	0.01	0.00
	Contribution rate	84.85	8.51	5.20	1.45
2022	NDVI	-0.15	-0.25	-0.92	0.26
	LST	-0.85	0.53	0.00	0.02
	WET	0.45	0.73	-0.37	-0.37
	NDBSI	-0.25	-0.36	-0.11	-0.89
	Feature value	0.04	0.01	0.00	0.00
	Contribution rate	69.46	22.44	5.99	2.11

Table 3. Principal component analysis results.

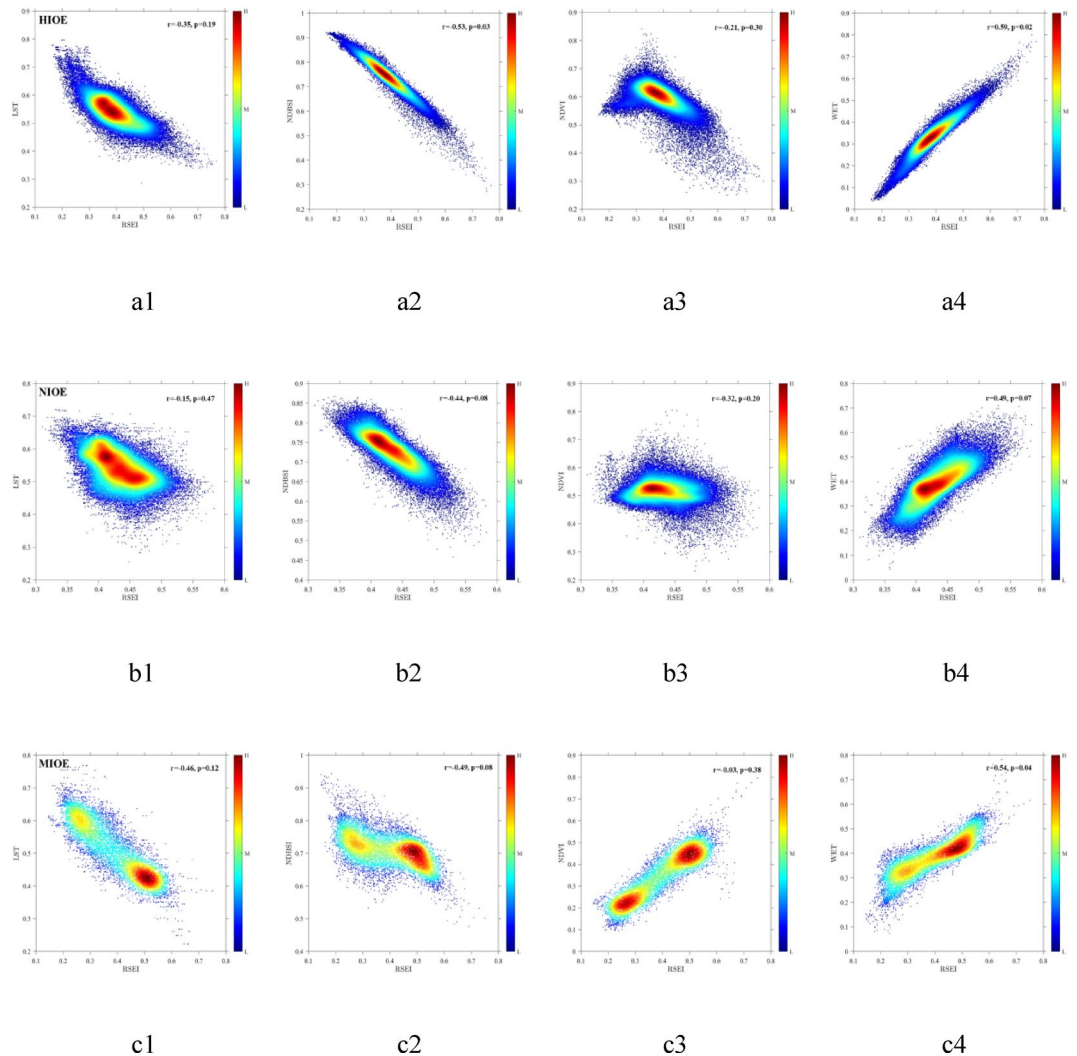


Fig. 3. Scatter plots of RSEI with LST, NDBSI, NDVI, and WET (a. HIOE; b. NIOE; c. MIOE) (Version Origin 2024b; <https://www.originlab.com>).

of regions with lower RSEI values. In general, the ecological quality was worse in oasis regions with greater LST and NDBSI. This situation is observed on the western side of the HIOE in Fig. 4b1 and c1, as well as along the eastern and western boundary edges in Fig. 4b2 and c2.

The RSEI is divided into five classes based on previous research and the equal interval approach^{16,50}: Excellent (0.8–1.0), Good (0.6–0.8), Medium (0.4–0.6), Poor (0.2–0.4), and Bad (0–0.2). The majority of oases in the dry zone were categorized as Medium or Poor overall. In particular, there were 19.5% poor and 80.5% medium regions in the NIOE. According to the HIOE, 56.5% of regions were poor and 42.0% were medium. 49.4% of the MIOE was in poor regions, while 48.8% was in medium areas (Fig. 5).

Within the HIOE, the western regions exhibit the highest concentration of degraded zones, whereas the eastern regions maintain superior ecological quality. Poor-quality areas are mostly found in the NIOE around the western plain-hill transitional zones and along the Yellow River's main channel. The Gobi desert margins that encircle the irrigated areas are where the MIOE's degraded zones are most prevalent.

Spatiotemporal variation analysis of RSEI

Temporal variation analysis of RSEI

In the HIOE, NIOE, and MIOE, the RSEI variation patterns are largely consistent. While the RSEI in the NIOE displays a fluctuating rising trend and a fluctuating downward trend in the MIOE, the RSEI in the HIOE stays in a state of fluctuating equilibrium. The interannual change rates of the RSEI for the three major oases—HIOE, NIOE, and MIOE—are -0.0062 a^{-1} , 0.0066 a^{-1} , and -0.0003 a^{-1} , respectively (Fig. 6a). According to the four RSEI indicators (Fig. 6b–e), WET shows a rising tendency, whereas LST, NDBSI, and NDVI all indicate a declining trend. The three regions' respective fall rates in the LST indicator are -0.0019 a^{-1} , -0.0031 a^{-1} , and -0.0035 a^{-1} . The drop rates are -0.0051 a^{-1} , -0.0062 a^{-1} , and -0.0012 a^{-1} for the NDBSI indicator. The fall rates for the NDVI index are -0.0026 a^{-1} , -0.0056 a^{-1} , and -0.0085 a^{-1} . In contrast, the increasing rates in the WET indicator are 0.0006 a^{-1} , 0.0006 a^{-1} , and 0.0012 a^{-1} , in that order. According to the variation trends of the four indicators and the

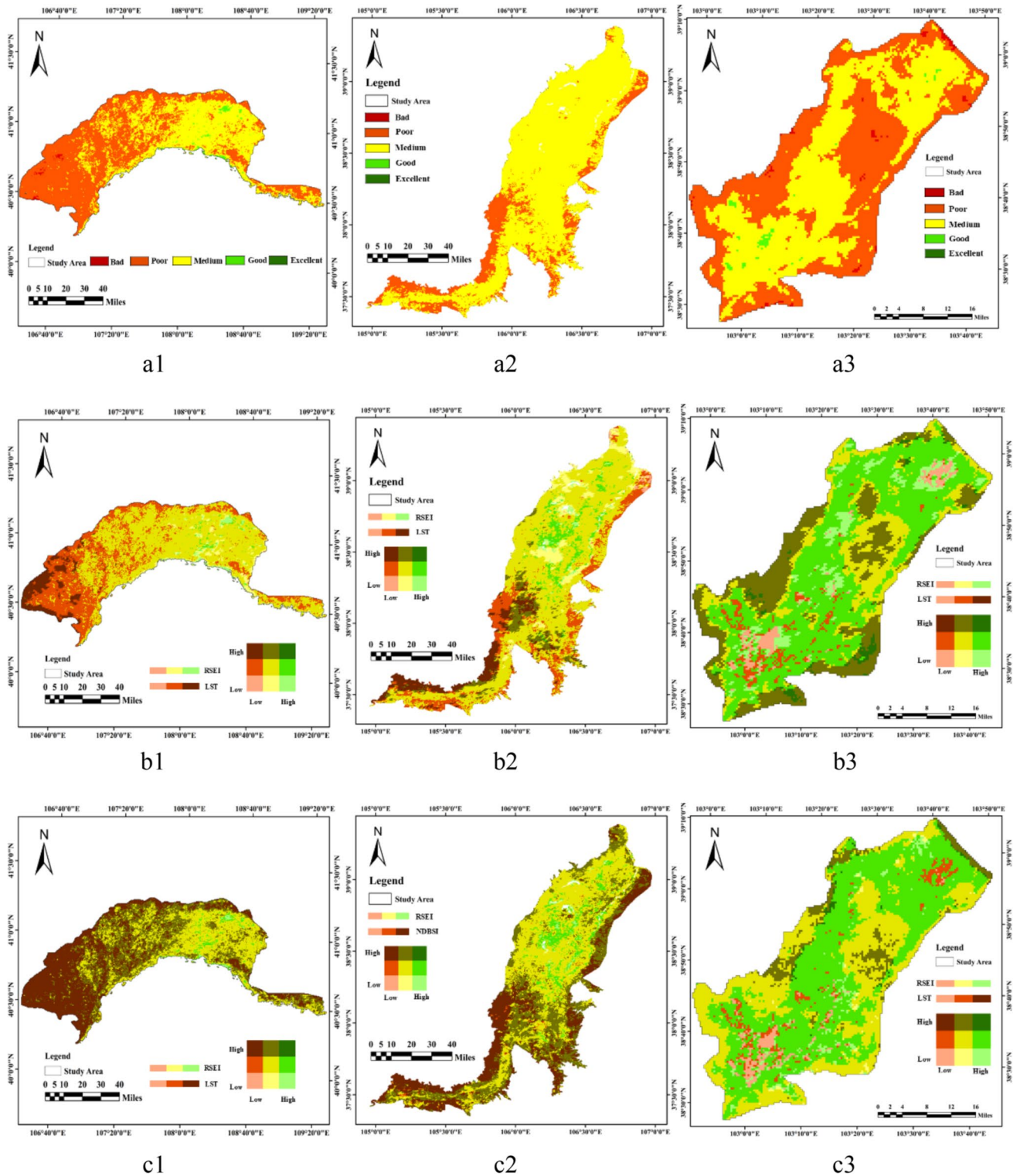


Fig. 4. RSEI and bivariate spatial distribution (a. RSEI spatial distribution; b. RSEI and LST; c. RSEI and NDBSI; d. RSEI and NDVI; e. RSEI and WET) (version QGIS 3.28; <https://qgis.org/en/site/forusers/download.html>).

RSEI, the decline in NDVI in the NIOE region has not resulted in a corresponding decrease in RSEI, indicating that EEQ does not exhibit a simple linear relationship with NDVI. A comparison of the trends of the four indicators and RSEI between NIOE and HIOE shows that the growth rate of WET in NIOE is higher than that in HIOE, while the decline rates of LST, NDVI, and NDBSI in NIOE are all greater than those in HIOE. This

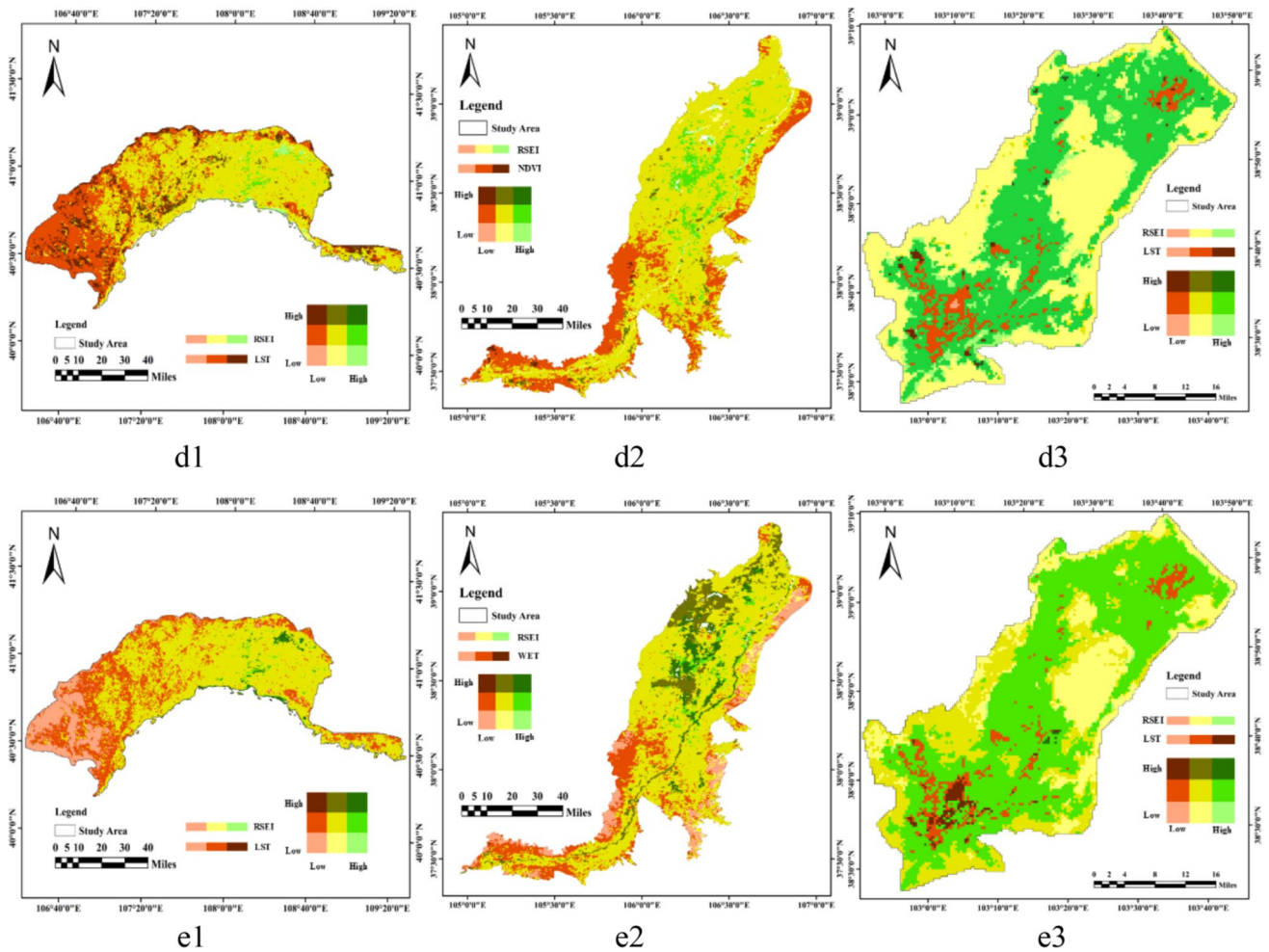


Fig. 4. (continued)

comparative analysis suggests that WET is positively correlated with RSEI, whereas the combined effects of LST, NDVI, and NDBSI are negatively correlated with RSEI.

Spatial variation analysis of RSEI

Significant regional variations in the shifting ecological quality patterns in arid oasis regions are revealed by trend analysis (Fig. 7). In RSEI, the HIOE shows a trend of degradation, with 61.4% of the region degrading, 31.5% improving, and 7.1% staying the same. The HIOE's RSEI changes between 2000 and 2022 were mostly characterized by degradation, which accounted for 61.4% of the total area. Significantly, the ecological quality of the piedmont buffer zones trended upward, but the areas near the Yellow River's main course had indications of mild deterioration. With 89.9% of the region improving, 7.8% degrading, and 2.3% staying the same, the NIOE indicates an improving trend in RSEI. The RSEI changes in the NIOE from 2000 to 2022 were mostly characterized by modest improvement, making up 82.2% of the entire region. The whole study area has seen this improvement, but there are indications of deterioration in the Shahu region and the Yinchuan metropolitan area. According to the MIOE, the RSEI is trending downward, with 53.7% of the region degrading, 38.3% improving, and 8.1% staying the same. Mild deterioration accounted for 48.5% of the total area and was the main characteristic of the RSEI changes in the MIOE between 2000 and 2022. While the oasis's border sections had indications of improved ecological quality, the oasis' middle region suffered from modest deterioration.

Bivariate analysis reveals that while LST and NDBSI fall, regions with rising RSEI are often comparable to those with rising NDVI and WET. These regions are often complimentary to those where LST and NDBSI rise while NDVI and WET fall. Even if the NDVI is trending upward and the vegetation regeneration is quite robust in certain areas, including the western portion of the HIOE, soil moisture levels are somewhat declining and surface temperatures are still high. The regional EEQ is somewhat degraded as a result.

RSEI sustainability and future trend analysis

The RSEI from 2000 to 2022 is shown in Fig. 8. The Hurst index ranges from 0.16 to 0.75. This implies that the trend of RSEI change is essentially unsustainable. Since unsustainable regions make up 77.8% of the total, it is likely that the present EEQ trend will not continue and that future trends will diverge from the current ones.

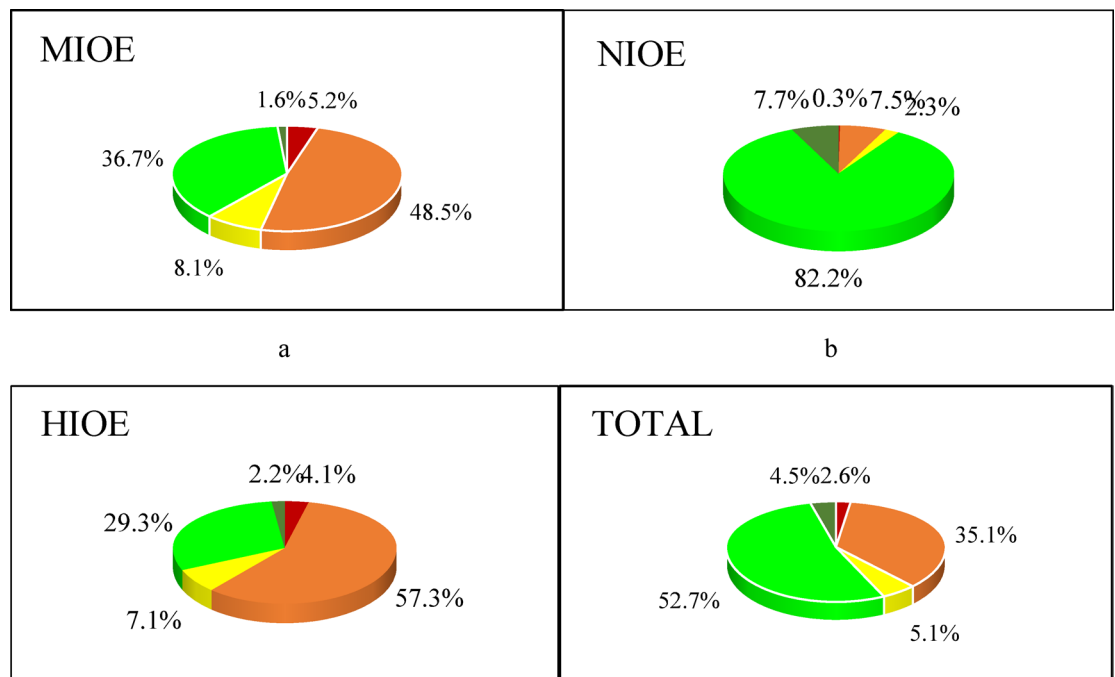


Fig. 5. Spatial coverage of medium and poor RSEI grades in irrigated oases across arid regions.

Subregional variations indicate unsustainability: HIOE, NIOE, and MIOE have unsustainable proportions of 90.6%, 86.1%, and 56.7%, respectively.

In order to forecast future trends, this study superimposes spatial change patterns on top of the Hurst index. The three irrigation oasis' improvement tendencies are erratic. Taking everything into account, the tendency toward future change aligns with the prior pattern, which was primarily focused on improvement. However, if ecological protection and sustainable management techniques are not implemented, further degradation may be possible. Of these, 86.8% of the regions that have been improved thus far may degrade to varied degrees, making up 51.8% of the entire area (Table. 4).

In the meantime, 13.4% of the areas—or 8.0% of the entire area—will keep getting better. 17.6% of the existing degraded areas—or 7.1% of the overall area—will continue to deteriorate. However, in the future, 82.4% of the areas (or 33.2% of the total area) could go toward an improving trend. An additional 51.8% of the land is projected to shift from improvement to degradation—these areas are characterized by sparse vegetation cover, severe water resource issues, persistently low baseline levels of ecological quality, and minimal historical fluctuations, all of which contribute to future ecological degradation.

It has been noted that the RSEI of the MIOE and HIOE may increase in the future, whereas the RSEI of the NIOE may decline. In the NIOE, although most areas have shown a recent upward trend in RSEI, the relatively low Hurst index indicates that this positive gain is unsustainable. In contrast, while most areas in HIOE and MIOE have experienced a recent decline in RSEI, their low Hurst index suggests that the current ecological degradation is also unsustainable (Fig. 9).

RSEI influencing factor analysis

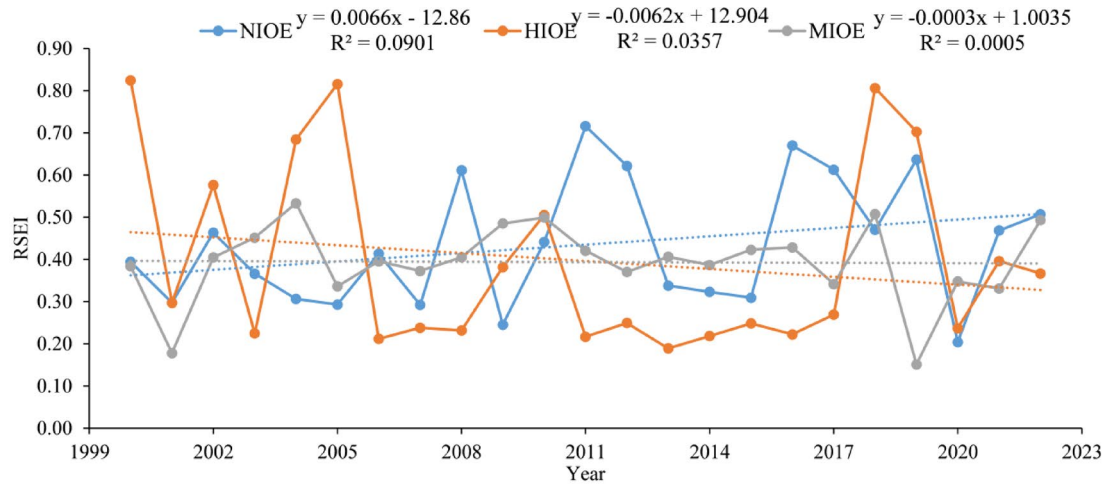
Accuracy evaluation of machine learning regression models

The contribution of each component to RSEI is not well represented by conventional linear regression models. Thus, a variety of machine learning models, such as RF, XGB, KNN, DT, LGB, and GBDT models, are constructed in this work. To choose the optimal model that can accurately capture the significance of the variables affecting RSEI changes, assessment measures such as MAE, MSE, and R² are employed (Fig. 10).

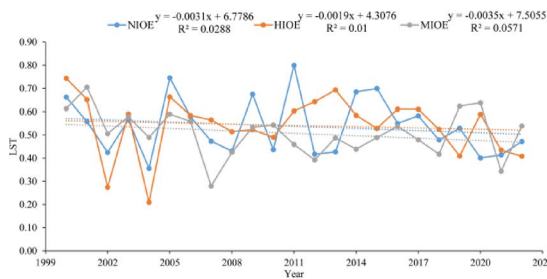
The radar map shows that RF's R² values for the three distinct irrigated oasis are far greater than those of other models, demonstrating its better generalization and forecast accuracy. However, in certain situations, XGB and LGB perform worse, maybe as a result of inadequate parameter adjustment or overfitting hazards. Additionally, RF performs better than other models in terms of MAE and MSE, exhibiting greater interpretability and stability. As a result, RF is chosen as the best model.

Interpretable machine learning model analysis

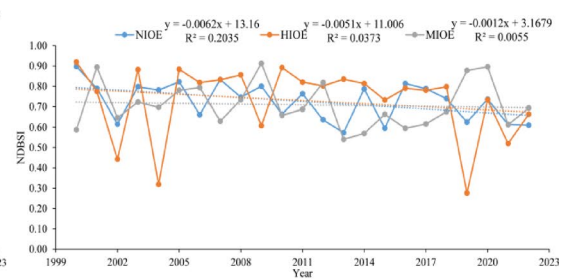
PRE is the most significant factor influencing RSEI across the three irrigation oases, according to the feature analysis bar chart (Fig. 11). The three oasis differ in the second, third, and fourth most important variables, though. The next most important components in the HIOE after PRE are IV, SMC, and PET. IV, FVC, and NL are the rankings in the NIOE. IV, PET, and FVC are the order in the MIOE. Notably, the second, third, and fourth variables' contributions are somewhat equal in the NIOE, while the disparities in these components' contribution rates are more noticeable in the other two oases. In all three oases, LUCC is also one of the least



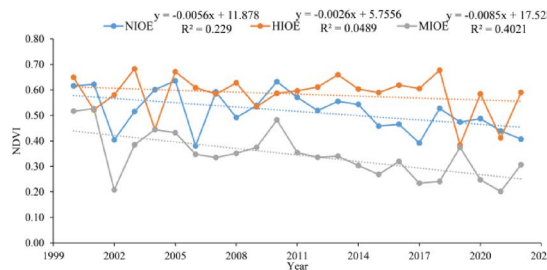
a



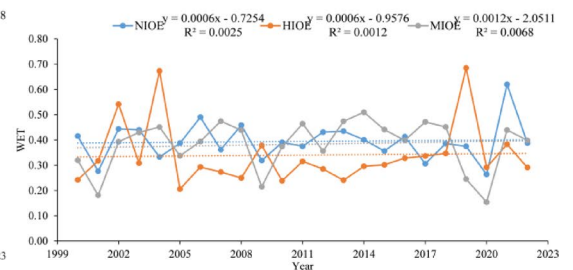
b



c



d



e

Fig. 6. Temporal trends of RSEI and the four indicators (a. RSEI trends in different arid oasis regions; b. LST; c. NDBSI; d. NDVI; e. WET).

significant contributors. Additionally, in two of the three oasis, POP and NL are among the least important parameters. According to these findings, human activity has a little effect on the total biological environment in oasis in dry regions, but climatic conditions have the greatest influence.

PRE is the most significant factor influencing the RSEI across the three irrigated oasis, as shown by the feature analysis bar chart (Fig. 11). The oasis differ in the second, third, and fourth most important variables, though. The influencing elements in the HIOE include IV, SMC, and PET in that order. They are IV, FVC, and NL in the NIOE. These include IV, PET, and FVC at the MIOE. Interestingly, the contribution rates of the NIOE's second, third, and fourth ranking criteria are comparable, whereas the rankings of the other two oases show more noticeable variations. Furthermore, POP and NL are among the least important elements in two of the oases, whereas LUCC routinely is among the worst three influencing factors in all three. According to

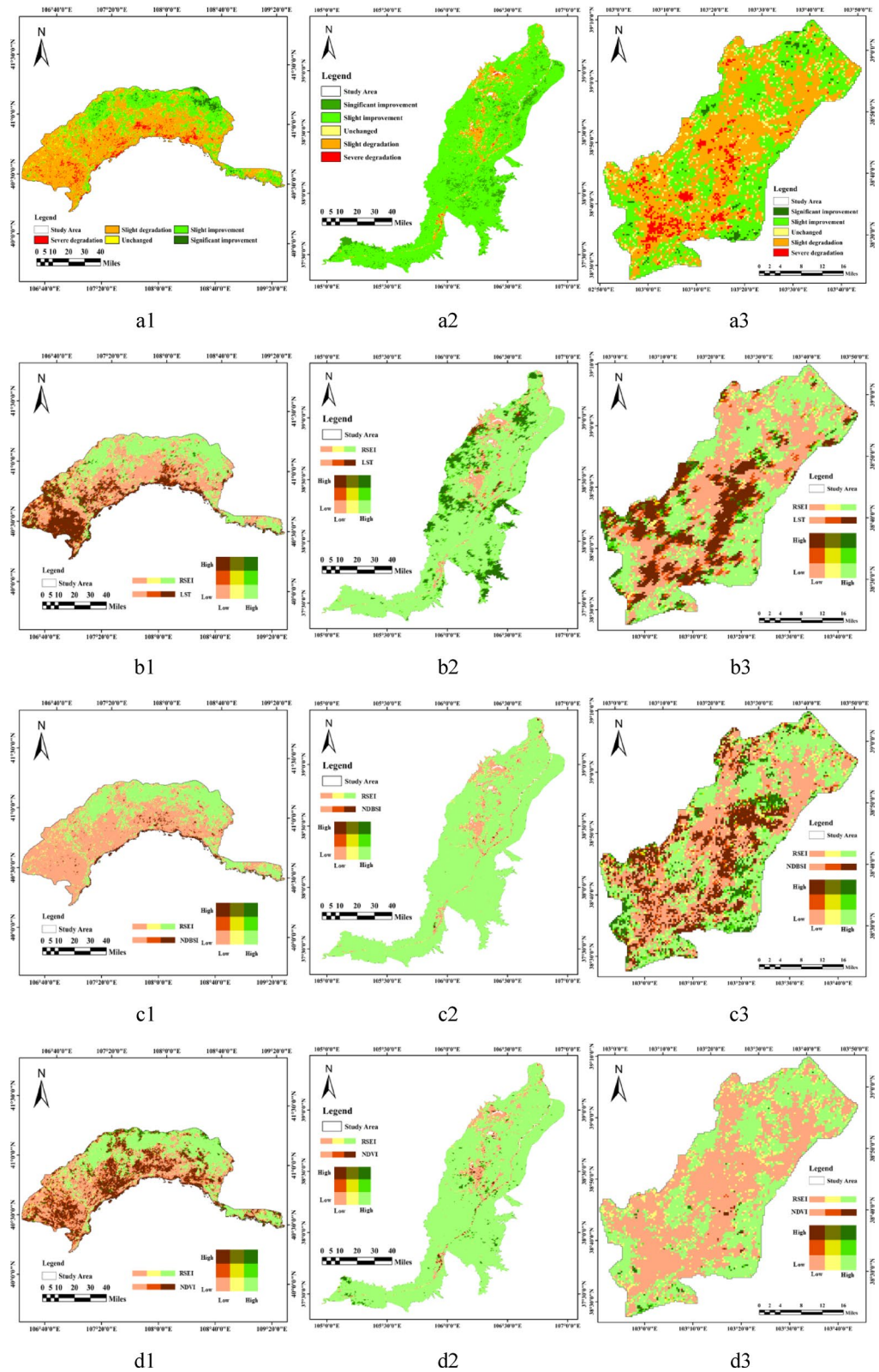


Fig. 7. Bivariate analysis of RSEI spatial trends and indicator component trends (a. Spatial distribution of RSEI spatial trends; b. Bivariate analysis of RSEI spatial trends and LST spatial trends; c. Bivariate analysis of RSEI spatial trends and NDBSI spatial trends; d. Bivariate analysis of RSEI spatial trends and NDVI spatial trends; e. Bivariate analysis of RSEI spatial trends and WET spatial trends.) (version QGIS 3.28; <https://qgis.org/en/site/forusers/download.html>).

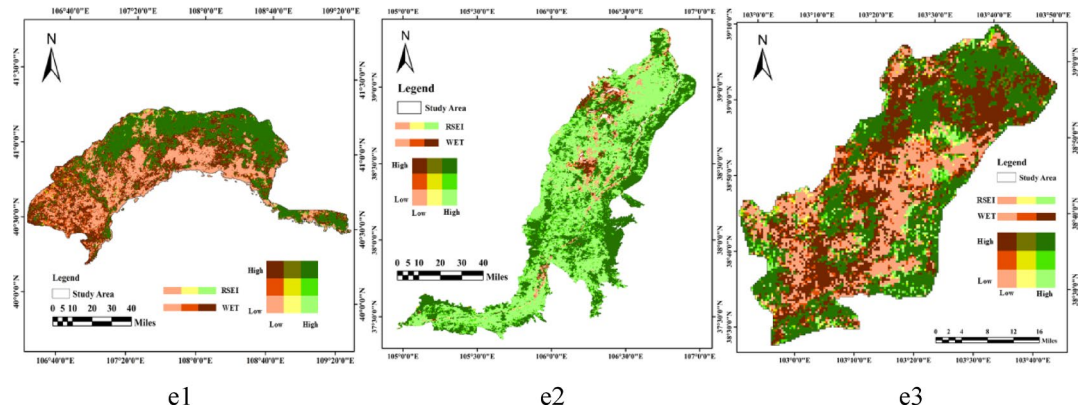


Fig. 7. (continued)

these results, human activities have a very minor influence on the total EEQ in desert oasis, whereas climatic conditions have the most impact. Water resources are a major factor in EEQ in all three regions, as seen in Fig. 8a–c. PRE mostly has a favorable effect on RSEI; some SHAP values are higher than 0.3. When PRE is low, it has a large negative influence on RSEI, as seen by the majority of related SHAP values being negative. The SHAP value rises and progressively becomes positive as PRE grows. In this study, the three irrigation oases were treated as an integrated system. Remote-sensing imagery of soil salinization (SI) for the three oases was retrieved from the GEE platform, and the InVEST model was employed to quantify the interannual dynamics of EEQ in conjunction with annual IV and PRE. As illustrated in Fig. 14, the aggregated EEQ and SI of the three oases exhibit concordant temporal trends, both declining with decreases in PRE and IV. Notably, in 2010 the EEQ did not rise despite simultaneous increases in PRE and IV. To further examine this anomaly, the R model was reapplied: PRE and IV values within this range were interpolated and discretized, and the EEQ trajectory was re-predicted and compared with the SI trend. The analysis indicates that when PRE and IV reach approximately 164 mm and 1218 mm, respectively, the SHAP values attain a peak and subsequently decline. These results support the conclusion that precipitation and irrigation jointly regulate regional RSEI and that excessive precipitation and irrigation can induce soil salinization, ultimately leading to a deterioration of RSEI⁵¹.

Figures 12a–c and 13 show how each element affects various oases and how they interact with one another. Model predictions are most affected by the features near the top of the plots. The mean absolute SHAP interaction values over all sample points indicate the overall significance of each component. According to the study, fluctuations in EEQ are mostly caused by interactions between meteorological conditions and irrigation water. The top three interactions in the HIOE area are IV and PRE, PET and SMC, and PRE and PET. They are PRE and IV, FVC and PRE, and PRE and NL in the NIOE area. They are IV and FVC, IV and PRE, and PRE and PET in the MIOE area.

Discussion

RSEI distribution and changes in arid region oases

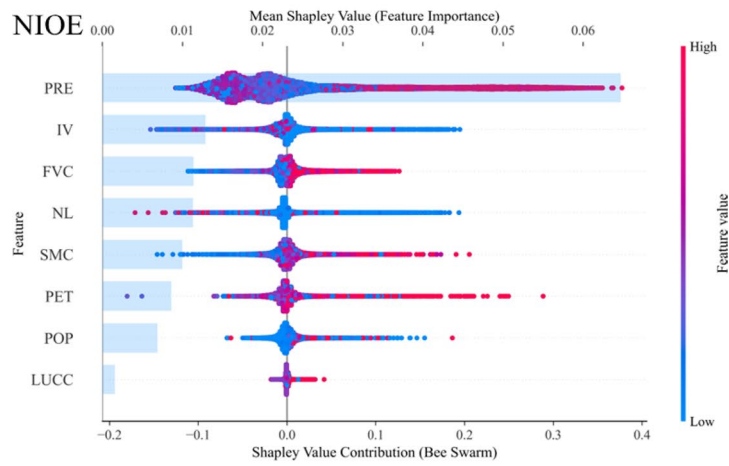
The RSEI is a composite metric derived from regional greenness, surface temperature, humidity, and dryness. Areas with relatively high EEQ are typically characterized by low surface temperature and dryness, together with high vegetation cover and soil moisture⁵². Our findings are broadly consistent with earlier studies⁵³, which underline the importance of vegetation and precipitation in ecological restoration and conservation. Notably, significant variations in EEQ were observed when the annual irrigation water volume approached ~1218 mm. China remains one of the countries most severely affected by desertification, which is a primary driver of low EEQ in the study region⁵⁴. All three irrigation oases—particularly the HIOE—contain extensive desertified land. In agreement with previous research, the regional RSEI has shown an overall upward trend⁵⁵. However, the HIOE displays a declining RSEI because the area of degradation exceeds that of improvement, even though many studies have reported an increase in vegetation cover. Rapid urbanization in arid zones has intensified water-resource exploitation, hindered vegetation recovery, and triggered ecological degradation, which likely explains this apparent discrepancy. A similar pattern is evident in the NIOE.

Interestingly, the observed trends in surface dryness and temperature diverge from the overall RSEI trajectory. In the HIOE, the rise in atmospheric humidity has not been sufficient to offset the negative impacts of increasing dryness, warming, and decreasing greenness, resulting in a net decline in RSEI. This underscores the necessity of comprehensive, long-term ecological monitoring. Areas of RSEI deterioration are concentrated in zones of rapid urban expansion and economic growth, where land-use change disrupts landscape continuity, alters the radiative and physiological properties of terrestrial ecosystems, raises surface temperatures, and ultimately degrades ecological environmental quality⁵⁶.

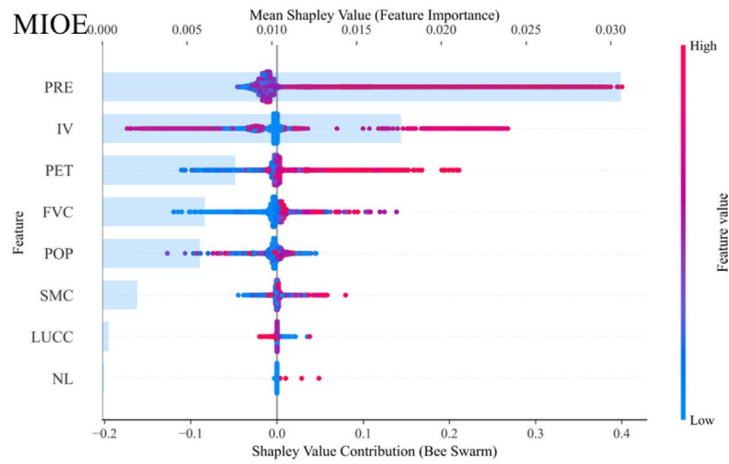
It is important to note that some explanatory factors used in our driver analysis—such as PET, SMC, and FVC—are correlated with the remote-sensing indicators that constitute the RSEI. We therefore interpret these variables not as independent measurements of the same state but as process-oriented drivers that modulate ecological quality. For example, PET represents the atmospheric demand for water and governs surface energy balance; SMC reflects subsurface hydrological dynamics; and FVC captures vegetation response to both climate



a



b



c

Fig. 8. Proportions of RSEI variation trends in different regions (Dark green, light green, yellow, orange, and red represent significant improvement, slight improvement, no change, slight deterioration, and severe degradation, respectively).

	MIOE (%)	NIOE (%)	HIOE (%)	Total (%)
Sustained improvement	16.1	12.3	2.1	8.0
Degradation-to-improvement transition	30.7	7.2	57.7	33.2
Continuing degradation	27.3	1.6	7.4	7.1
Improvement-to-degradation transition	26.0	78.9	32.8	51.8

Table 4. Classification results of trend variations across subregions.

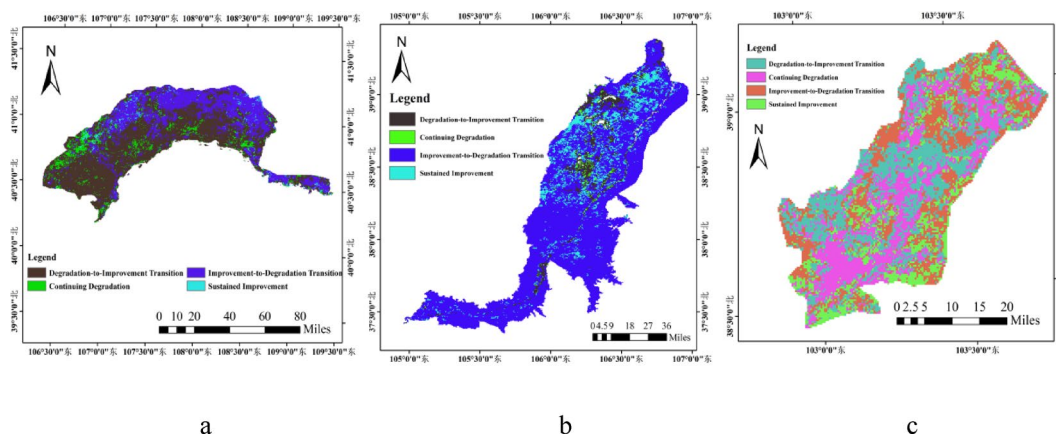


Fig. 9. Hurst index distribution of RSEI in arid oasis regions (a. HIOE; b. NIOE; c. MIOE). (version QGIS 3.28; <https://qgis.org/en/site/forusers/download.html>)

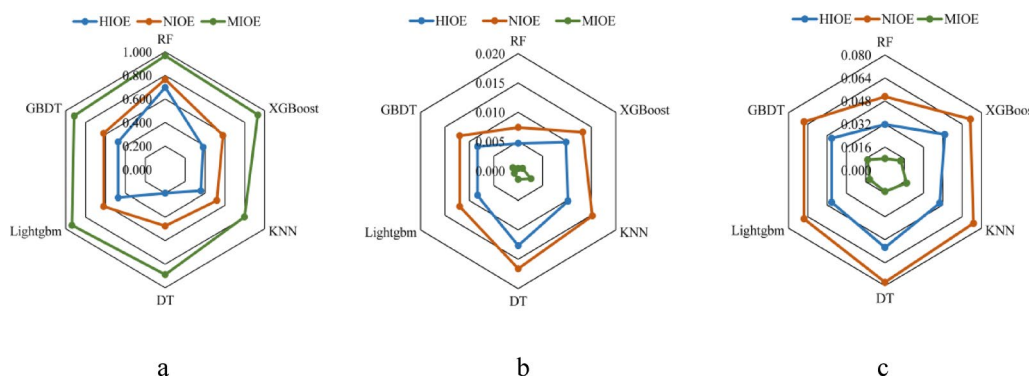


Fig. 10. Radar chart of machine learning model accuracy (a. R^2 ; b. MSE; c. MAE).

variability and human irrigation. By treating these metrics as external climatic and hydrological controls rather than as simple repetitions of the RSEI components, we reduce the risk of circular reasoning and highlight their mechanistic roles in shaping spatiotemporal changes in ecological environmental quality.

The impact of climatic factors and iv on the rsei of arid region oases

RSEI fluctuations represent a complex and dynamic process shaped by the combined effects of human activities and natural forces, with both positive and negative consequences for the ecological environment. Regional heat, humidity, dryness, and greenness respond to a variety of external drivers, including climate variability and land-use change. Because many environmental and anthropogenic factors covary and exert nonlinear effects on RSEI, it is inherently difficult to isolate the precise contribution of each driver. To address this challenge, the present study employed explainable machine-learning models to analyze large-scale datasets, enabling the capture of intricate interactions between influencing variables and RSEI and providing quantitative estimates of their relative importance. This framework reveals not only the magnitude but also the direction of each driver's effect. Our results indicate that PRE, FVC, and IV are the dominant contributors to RSEI variation, with precipitation exerting the greatest influence. These findings are consistent with earlier research in arid and semi-arid regions³⁸. Because irrigation oases are located in water-limited landscapes with low annual rainfall, variability

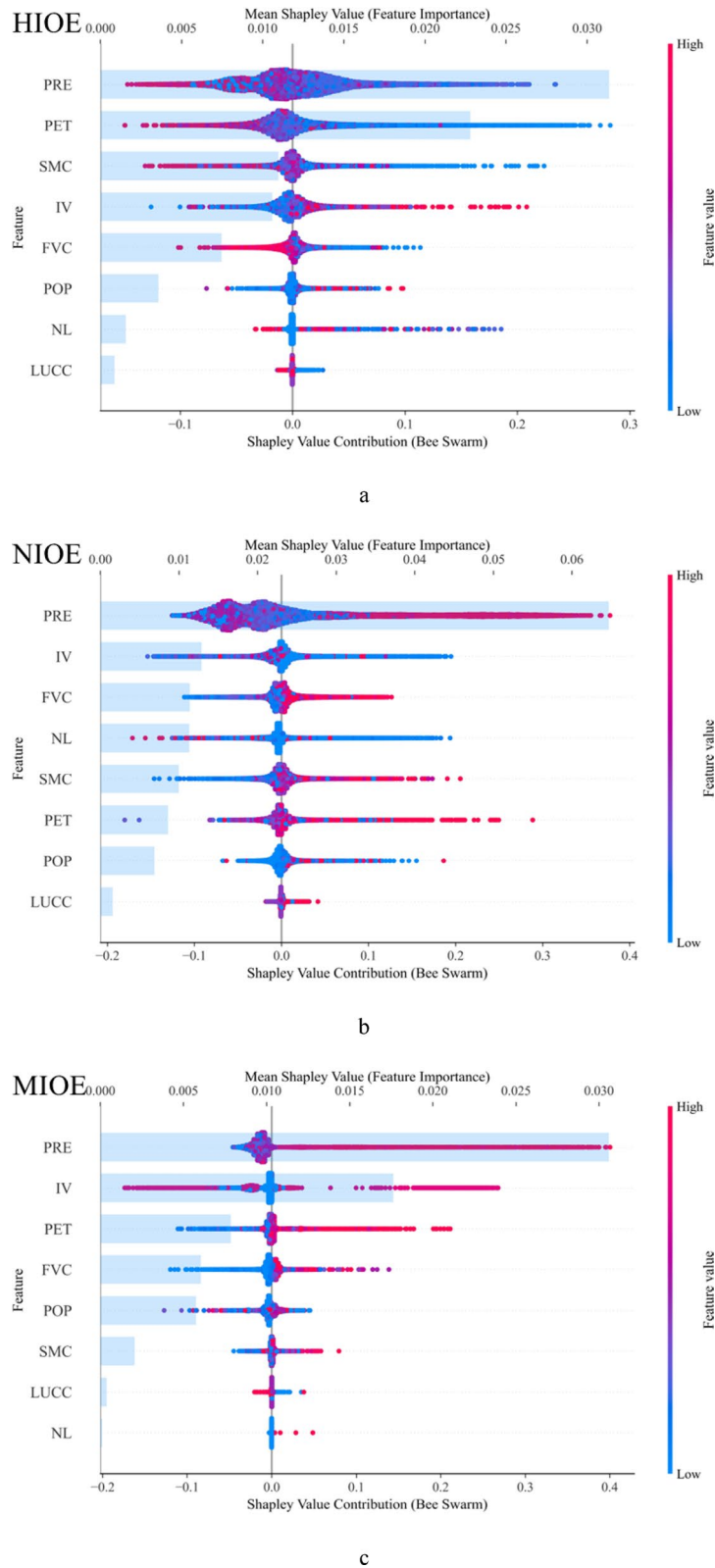
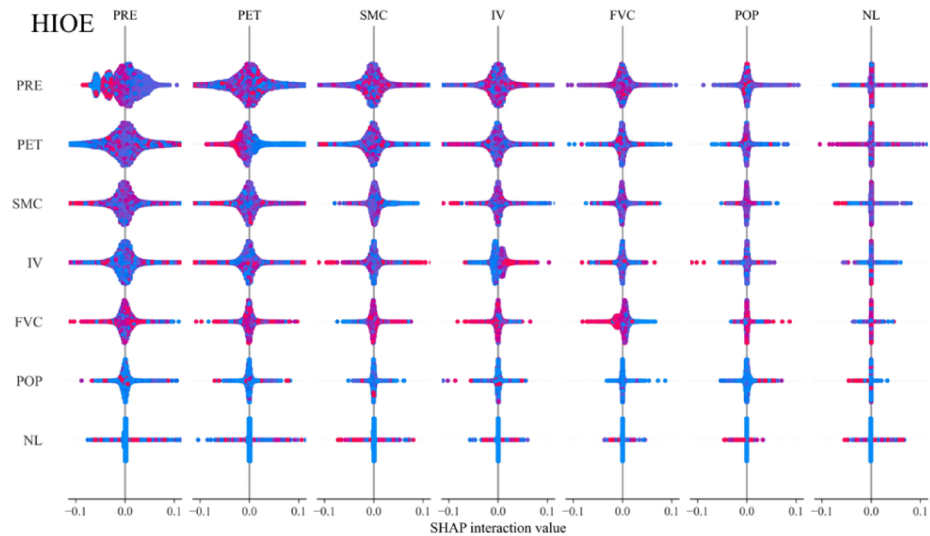


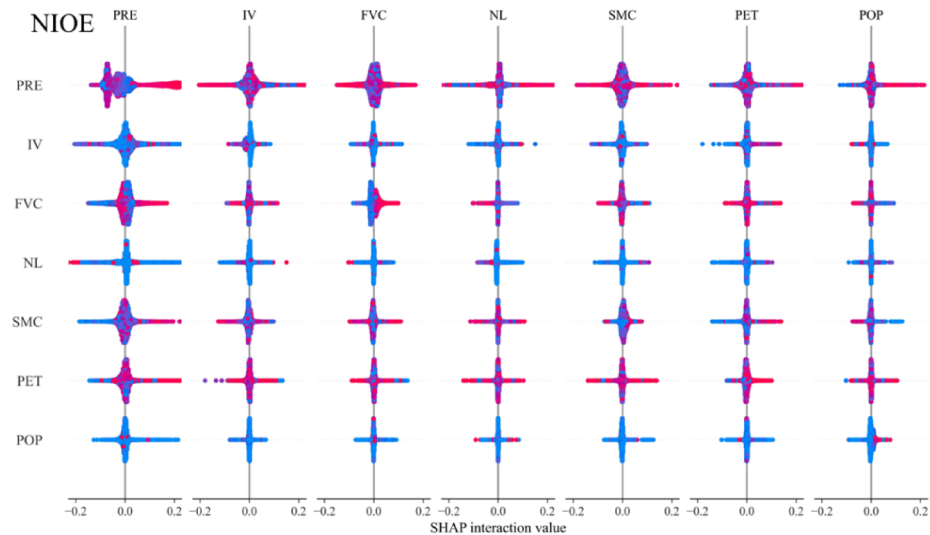
Fig. 11. SHAP bar plot and cluster plot (a. HIOE; b. NIOE; c. MIOE).

in precipitation strongly regulates vegetation dynamics and ecosystem processes. Under global climate change, water availability remains the primary constraint on vegetation and ecosystem functioning⁵⁷.

It is worth noting, however, that higher precipitation does not uniformly lead to increased RSEI. In some locations, abundant rainfall or intensive irrigation can induce soil salinization, which negatively affects



a



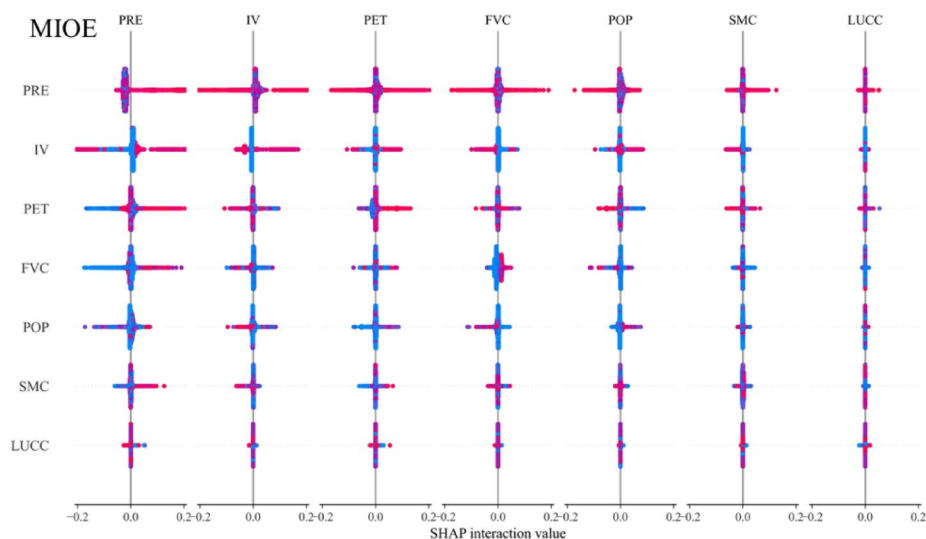
b

Fig. 12. SHAP interaction plot (a. HIOE; b. NIOE; c. MIOE).

ecological environmental quality⁵². The net impact of irrigation and precipitation on RSEI is therefore mediated by changes in soil moisture and salt content. When annual irrigation water volume and precipitation approach approximately 1218 mm and 164 mm, respectively, their initially positive effects may shift to inhibition⁵⁴. Although variables such as FVC share conceptual overlap with the remote-sensing indicators used to construct the RSEI, we interpret them here as process-oriented drivers rather than redundant measurements. FVC captures vegetation's ecological response to climate variability and human irrigation, while PRE and IV represent exogenous hydrological inputs. By emphasizing their mechanistic role in regulating soil water balance, energy fluxes, and vegetation growth, our analysis reduces the risk of circular reasoning and highlights how these drivers exert independent influences on the spatiotemporal variability of ecological environmental quality.

Limitations and future prospects

This study investigated the spatiotemporal dynamics of EEQ across three major irrigation oases from 2000 to 2022 using the RSEI on the GEE platform. Interpretable machine-learning models were applied to identify and quantify the key factors driving EEQ change. While the anticipated objectives were achieved, several limitations should be acknowledged.



C

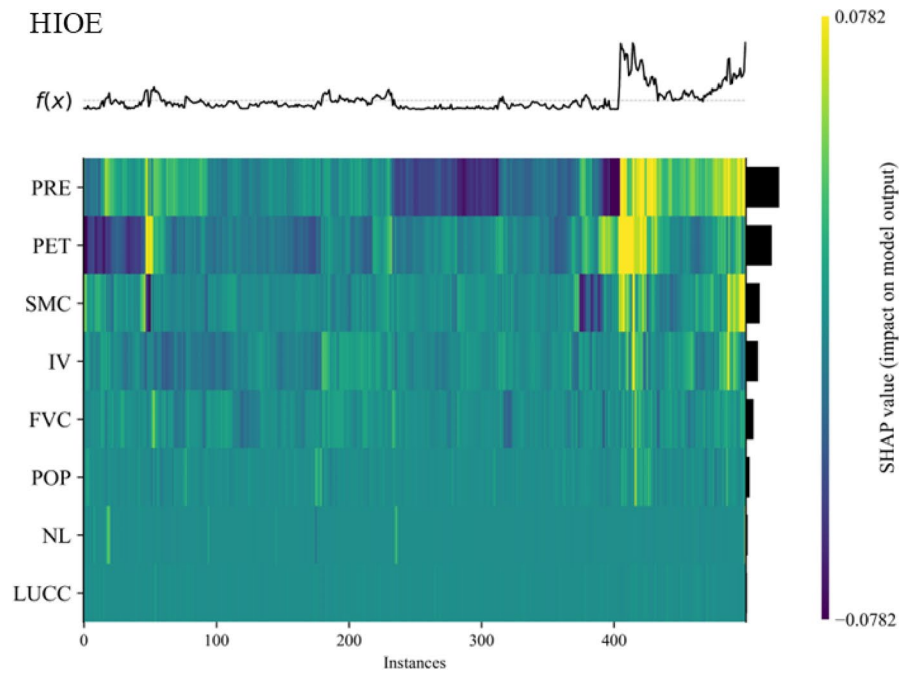
Fig. 12. (continued)

First, the indicators used to assess ecological quality remain inherently limited given the complexity and heterogeneity of ecosystems. Our RSEI-based analysis considered only temperature, humidity, dryness, and greenness. Region-specific stressors—such as explicit indices of desertification or soil salinization—were not included and could be incorporated in future work to capture additional ecological dimensions.

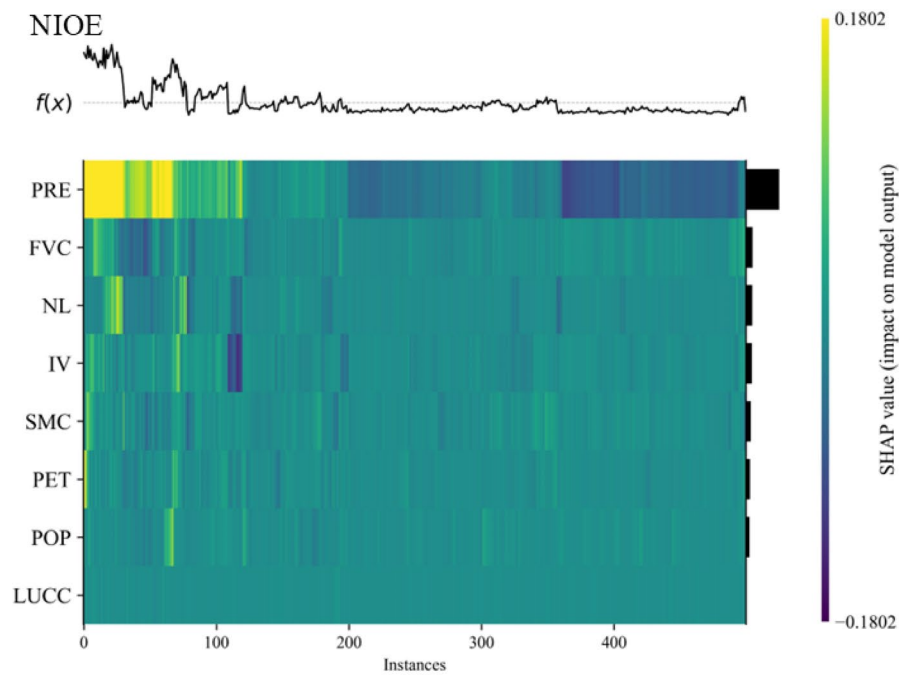
Second, although interpretable machine learning enabled the estimation of factor magnitudes, thresholds, and interactions, model performance may have been affected by spatially uneven sample sizes, intrinsic geographic heterogeneity, sensitivity to data noise, and variations in data quality. Future improvements could draw on advanced feature-selection strategies, data augmentation, ensemble modeling, and hyperparameter optimization to enhance robustness and predictive skill.

Third, while variables such as FVC are conceptually related to the remote-sensing indicators that constitute the RSEI, in this study they were treated as process-oriented drivers—representing ecological responses to hydrological and climatic variability—rather than as redundant measurements. This distinction reduces the risk of circular reasoning and clarifies their mechanistic role in shaping EEQ dynamics.

Finally, integrating machine-learning approaches with geospatial process-based models offers a promising but still developing avenue for building a more comprehensive framework to evaluate ecological environmental quality. Further research is needed to refine such hybrid methods and to better represent the spatial heterogeneity of interacting natural and anthropogenic drivers.

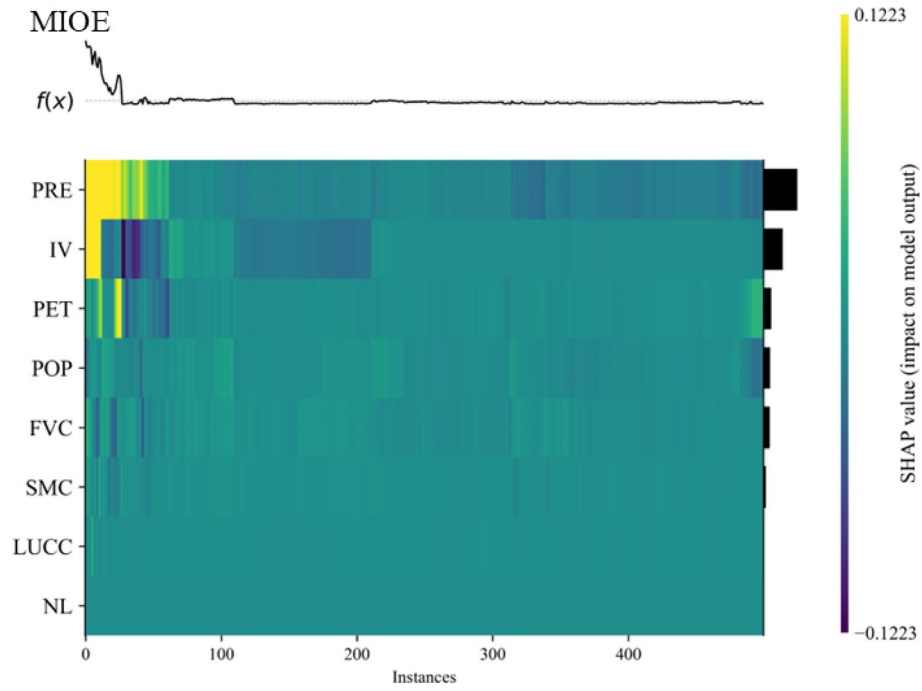


a



b

Fig. 13. SHAP heatmap (a. HIOE; b. NIOE; c. MIOE).



c

Fig. 13. (continued)

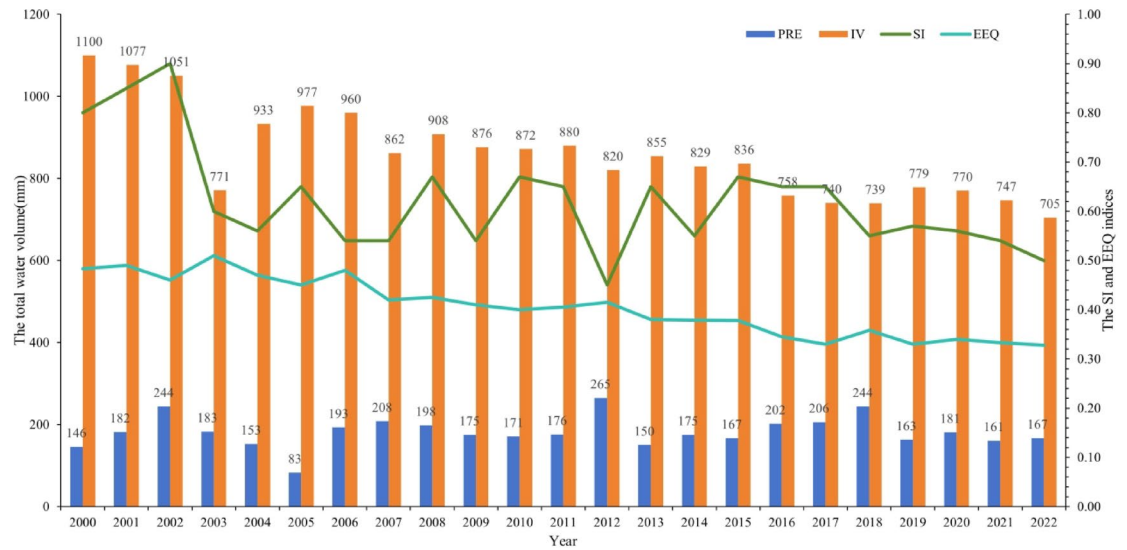


Fig. 14. Graph of SI and trends in EEQ changes.

Data availability

The datasets generated during the current study are available from the corresponding author on reasonable request.

Received: 9 May 2025; Accepted: 19 November 2025

Published online: 10 December 2025

References

- Liu, X., Li, H. K., Zhou, Y. B. & Wang, X. L. Spatiotemporal dynamics of vegetation net primary productivity in Chinese ecological function conservation areas: The influences of climate and topography. *J. Nat. Conserv.* **84**, 1617–1381. <https://doi.org/10.1016/j.nc.2025.126846> (2025).
- Lu, F. Y. et al. Assessment of ecological environment quality and their drivers in urban agglomeration based on a novel remote sensing ecological index. *Ecol. Ind.* **170**, 1470–2160. <https://doi.org/10.1016/j.ecolind.2025.113104> (2025).
- Chen, Q. et al. A review of emission metrics GWP and GTP. *Clim. Change Res.* **21**(01), 69–77 (2025).
- IPCC, Climate Change 2021-The Physical Science Basis Working Group I Contribution to the Sixth Assessment Report of the Intergovernmental Panel on Climate Change. Cambridge University Press, Cambridge. <https://doi.org/10.1017/9781009157896> (2023).
- An, X. I., Ruhan, A., Ziyang, S. U. & Xiaohan, S. U. Assessment of ecological environment in arid region based on the improved remote sensing ecological index: A case study of Wuchuan Country, Inner Mongolia at the northern foot of Yin Mountains. *Chin. J. Appl. Ecol.* **35**(7), 1907–1914 (2024).
- Raj, P. et al. Conceptualization of arid region radioecology strategies for agricultural ecosystems of the United Arab Emirates (UAE). *Sci. Total Environ.* **832**, 0048–9697. <https://doi.org/10.1016/j.scitotenv.2022.154965> (2022).
- Chang, K. F., Lin, C. T. & Bin, Y. Q. Harmony with nature: Disentanglement the influence of ecological perception and adaptation on sustainable development and circular economy goals in country. *Heliyon* **10**(4), e26034. <https://doi.org/10.1016/j.HELIYON.2024.E26034> (2024).
- Yu, H. L. et al. Sunflower LAI inversion based on unmanned aerial vehicle remote sensing data and machine learning. *Transac. Chin. Soc. Agric. Mach.* **56**(01), 356–365 (2024).
- Li, X. Y., Xin, Z. B., Yang, J. L. & Liu, J. H. The spatiotemporal changes and influencing factors of vegetation NDVI in the Hehuang Valley of Qinghai Province from 2000 to 2020. *J. Soil Water Conserv.* **38**(1), 79–90 (2024).
- Ma, X. B., Zhang, J. H., Guo, J. L., Yang, J. L. & Wang, J. W. Traps and improvements of PSR model: An eco-environmental perspective. *Acta Ecol. Sin.* **44**(12), 4923–4932. <https://doi.org/10.20103/j.stxb.202303290612> (2024).
- Lyu, K., Tian, J., Zheng, J., Zhang, C. & Yu, L. Evaluation of water-carbon-ecological footprint and its spatial-temporal changes in the North China Plain. *Land*. **13**, 1327. <https://doi.org/10.3390/land13081327> (2024).
- Lu, F., Zhang, C., Jia, T., Huang, Z. & Xu, M. Spatio-temporal evolution characteristics and driving mechanisms of urban ecological resilience in the Yangtze River economic belt. *Environ. Sci.* <https://doi.org/10.13227/j.hjck.202407165> (2024).
- Yao, Y., Wang, S., Zhou, Y., Liu, R. & Han, X. The application of ecological environment index model on the national evaluation of ecological environment quality. *Remote Sens. Inf.* **27**, 93–98. <https://doi.org/10.3969/j.issn.1000-3177.2012.03.016> (2012).
- Zhang, F. et al. Ecological vulnerability assessment based on multi-sources data and SD model in Yinma River Basin, China. *Ecol. Model.* **349**, 0304–3800. <https://doi.org/10.1016/j.ecolmodel.2017.01.016> (2017).
- Xu, H. A remote sensing urban ecological index and its application. *Acta Ecol. Sin.* **33**(24), 7853–7862. <https://doi.org/10.5846/stxb20-1208301223> (2013).
- Cao, Z. et al. Space-time cube uncovers spatiotemporal patterns of basin ecological quality and their relationship with water eutrophication. *Sci. Total Environ.* **916**, 170195. <https://doi.org/10.1016/j.scitotenv.2024.170195> (2024).
- Xu, Y., Yang, X., Xing, X. & Wei, L. Coupling eco-environmental quality and ecosystem services to delineate priority ecological reserves-A case study in the Yellow River Basin. *J. Environ. Manag.* **365**, 121645. <https://doi.org/10.1016/j.jenvman.2024.121645> (2024).
- Li, S. Z. et al. Study on the ecological environment quality change in Hetao irrigation area with remote sensing ecology index. *Ecol. Sci.* **41**(3), 156–165. <https://doi.org/10.14108/j.cnki.10088873.2022.03.018> (2022).
- Wang, Z. W., Chen, T., Zhu, D. Y., Jia, K. & Plaza, A. RSEIFE: A new remote sensing ecological index for simulating the land surface eco-environment. *J. Environ. Manag.* **326**, 0301–4797. <https://doi.org/10.1016/j.jenvman.2022.116851> (2023).
- Wang, Y. Study on Ecological Security and Groundwater Level Regulation in Arid Areas. *China Institute of Water Resources and Hydropower Research.* **58**(1), 132–142 (2020).
- Tian, Y. C., Yang, T. & Xu, X. Temporal and spatial distribution characteristics and influencing factors of net primary productivity of vegetation in typical basin entering the sea in Beibu Gulf. *Ecol. Environ. Sci.* **30**(50), 938–948. <https://doi.org/10.16258/j.cnki.1674-5906.2021.05.006> (2021).
- Song, J. X. et al. Identifying the hotspots of nitrate leaching and its key driving factors in the Yellow River Delta using DNDC model. *J. Environ. Manag.* **373**, 0301–4797. <https://doi.org/10.1016/j.jenvman.2024.123533> (2024).
- Zhang, X. et al. Interpretable machine learning models for crime prediction. *Comput. Environ. Urban. Syst.* **94**, 101789. <https://doi.org/10.1016/j.compenvurbsys.2022.101789> (2022).
- Wang, Q. Z. Assessment of the impact of ecological and hydrological processes on agricultural water scarcity in the Shiyang River Basin. Lanzhou University, <https://doi.org/10.27204/d.cnki.glzhu.2024.000529> (2024).
- Zhang, Y., Chen, X. Y., Zhang, Y. & Wang, B. Quantitative contribution of climate change and vegetation restoration to ecosystem services in the Inner Mongolia under ecological restoration projects. *Ecol. Indic.* <https://doi.org/10.1016/j.ecolind.2025.113240> (2025).
- Zhai, Y. G., Wang, Y. S., Hao, L. & Qi, W. C. Medium- and long-term independent contributions of climate change, management measures and land conversion to vegetation dynamics and inspiration for ecological restoration in Inner Mongolia, China. *Ecol. Eng.* <https://doi.org/10.1016/j.ecoleng.2024.107504> (2025).
- Cao, Z. et al. Space-time cube uncovers spatiotemporal patterns of basin ecological quality and their relationship with water eutrophication. *Sci. Total Environ.* **916**, 170195. <https://doi.org/10.1016/j.scitotenv.2024.170195> (2024).
- Chen, H. et al. Effects of forest age and stand density on the growth, soil moisture content, and soil carbon content of Populus simoni plantations in the sandy area of western Liaoning Northeast China. *Sci Rep* **15**, 2499. <https://doi.org/10.1038/s41598-025-86215-4> (2025).
- Yu, K. et al. Analysis of vegetation coverage changes and driving forces in the source region of the yellow river. *Sci. Rep.* **15**, 22569. <https://doi.org/10.1038/s41598-025-06921-x> (2025).
- Yang, J. & Huang, X. The 30m annual land cover dataset and its dynamics in China from 1990 to 2019. *Earth Syst. Sci. Data* **13**, 3907–3925. <https://doi.org/10.5194/essd-13-3907-2021> (2021).
- Admas, H., Abbi, S. & Kassahun, T. Assessment of salt-affected soil extent and spatial variability using GIS and remote sensing in Asaita district Northeastern Ethiopia. *Sci. Rep.* **15**, 28038. <https://doi.org/10.1038/s41598-025-10969-0> (2025).
- Airken, M. & Li, S. The dynamic monitoring and driving forces analysis of ecological environment quality in the Tibetan Plateau Based on the google earth engine. *Remote Sens.* **16**, 682. <https://doi.org/10.3390/rs16040682> (2024).
- Zhang, Y., She, J., Long, X. & Zhang, M. Spatio-temporal evolution and driving factors of eco-environmental quality based on RSEI in Chang-Zhu-Tan metropolitan circle, central China. *Ecol. Indic.* **144**, 109436. <https://doi.org/10.1016/j.ecolind.2022.109436> (2022).
- Pan, Z. D., Wang, Y. F., Wang, K. Y., Zou, W. W. & Sun, Y. J. Ecological Quality assessment and driving analysis of Jiangle county based on modified remote sensing ecological index. *Environ. Sci.* <https://doi.org/10.13227/j.hjck.202408293> (2024).
- Xu, H., Wang, Y., Guan, H., Shi, T. & Hu, X. Detecting ecological changes with a remote sensing based ecological index (RSEI) produced time series and change vector analysis. *Remote Sens.* **11**, 2345. <https://doi.org/10.3390/rs11202-345> (2019).
- Yuan, B. et al. Spatiotemporal change detection of ecological quality and the associated affecting factors in Dongting Lake Basin, based on RSEI. *J. Clean. Prod.* **302**, 126995. <https://doi.org/10.1016/j.jclepro.2021.126995> (2021).

37. Zhu, Q. et al. Spatial variation of ecological environment quality and its influencing factors in Poyang Lake area. *Chin. J. Appl. Ecol.* **30**(12), 4108–4116 (2019).
38. Tang, Q. et al. Advancing ecological quality assessment in China: Introducing the ARSEI and identifying key regional drivers. *Ecol. Indic.* **163**, 112109. <https://doi.org/10.1016/j.ecolind.2024.112109> (2024).
39. Yang, X., Meng, F., Fu, P., Zhang, Y. & Liu, Y. Spatiotemporal change and driving factors of the eco-environment quality in the Yangtze River Basin from 2001 to 2019. *Ecol. Indic.* **131**, 108214. <https://doi.org/10.1016/j.ecolind.2021.108214> (2021).
40. Hurst, H. E. Long-term storage capacity of reservoirs. *Trans. Am. Soc. Civ. Eng.* **116**(1), 770–799. <https://doi.org/10.1061/TACEAT.0006518> (1951).
41. Rodriguez-Galiano, V., Sanchez-Castillo, M., Chica-Olmo, M. & Chica-Rivas, M. Machine learning predictive models for mineral prospectivity: An evaluation of neural networks, random forest, regression trees and support vector machines. *Ore Geol. Rev.* **71**, 804–818. <https://doi.org/10.1016/j.oregeorev.2015.01.001> (2015).
42. Lu, H. & Ma, X. Hybrid decision tree-based machine learning models for short-term water quality prediction. *Chemosphere* **249**, 126169. <https://doi.org/10.1016/j.chemosphere.2020.126169> (2020).
43. Wen, X., Xie, Y., Wu, L. & Jiang, L. Quantifying and comparing the effects of key risk factors on various types of roadway segment crashes with LightGBM and SHAP. *Accid. Anal. Prev.* **159**, 106261. <https://doi.org/10.1016/j.aap.2021.106261> (2021).
44. Muhammad, U. S. et al. Machine learning-based cotton yield forecasting under climate change for precision agriculture. *Smart Agric. Technol.* **12**, 101117. <https://doi.org/10.1016/j.atech.2025.101117> (2025).
45. Liu, X. Y., Zhang, M. L. & Ma, Z. M. Enhanced soil organic carbon mapping in Gannan's alpine meadows: A comparative analysis of machine learning models and satellite data. *Ecol. Indic.* **177**, 113800. <https://doi.org/10.1016/j.ecolind.2025.113800> (2025).
46. Parasar, P. & Krishna, A. P. Explainable AI-driven assessment of hydro climatic interactions shaping river discharge dynamics in a monsoonal basin. *Sci. Rep.* **15**, 27302. <https://doi.org/10.1038/s41598-025-13221-x> (2025).
47. Lv, X. et al. Maximizing multi-source data integration and minimizing the parameters for greenhouse tomato crop water requirement prediction. *Sci. Rep.* **15**, 29161. <https://doi.org/10.1038/s41598-025-12324-9> (2025).
48. Bofa, A. & Zewotir, T. Machine learning analysis of greenhouse gas sources impacting Africa's food security nexus. *Sci. Rep.* **15**, 28665. <https://doi.org/10.1038/s41598-025-14766-7> (2025).
49. Abdullah, H., Skidmore, A. K., Siegenthaler, A. & Neinavaz, E. High-Resolution prediction of soil pH in European temperate forests using Sentinel-2 and ancillary environmental data. *Sci. Rep.* **15**, 28509. <https://doi.org/10.1038/s41598-025-03942-4> (2025).
50. Awasthi, M. P. et al. Integrating multivariate statistical techniques and geochemical indices for water quality assessment in pond ecosystems of Kirtipur Municipality, Kathmandu Nepal. *Sustain. Water Resour. Manag.* **11**, 13. <https://doi.org/10.1007/s4-0899-024-01182-4> (2025).
51. Qin, Z. Y. et al. The characteristics and driving factors of soil salinisation in the irrigated area on the southern bank of the yellow river in inner Mongolia: A assessment of the Donghaixin irrigation district. *Agriculture* **15**(5), 566–566. <https://doi.org/10.3390/AGRICULTURE15050566> (2025).
52. Chang, C., Yang, G. Y., Li, S. Y., Wang, H. & Song, Y. M. Q. Spatial characteristics and critical groundwater depth of soil salinization in arid artesian irrigation area of northwest China. *Agric. Water Manag.* <https://doi.org/10.1016/J.AGWAT.2024.109196> (2024).
53. Zhang, L. Y. et al. Dynamic monitoring and drivers of ecological environmental quality in the Three-North region, China: Insights based on remote sensing ecological index. *Ecol. Inf.* **85**, 1574–9541. <https://doi.org/10.1016/j.ecoinf.2024.102936> (2025).
54. Dong, Y. Y. et al. Simulation and analysis of water balance effect and ecological impact of agricultural water saving in irrigated oasis of yellow river in Ningxia. *J. Basic Sci. Eng.* **32**(06), 1720–1739. <https://doi.org/10.16058/j.issn.1005-0930.2024.06.014> (2024).
55. Kang, S. et al. Spatiotemporal variation and driving factors of ecological environment quality on the loess plateau in China from 2000 to 2020. *Remote Sens.* **16**(24), 4778. <https://doi.org/10.3390/rs16244778> (2024).
56. Zheng, Z. H., Wu, Z. F., Chen, Y. B., Yang, Z. W. & Marinello, F. Exploration of eco-environment and urbanization changes in coastal zones: A case study in China over the past 20 years. *Ecol. Indic.* **2020**, 119. <https://doi.org/10.1016/j.ecolind.2020.106847> (2020).
57. Jiao, W. Z. et al. Observed increasing water constraint on vegetation growth over the last three decades. *Nat. Commun.* <https://doi.org/10.1038/s41467-021-24016-9> (2021).

Author contributions

LL.Z is responsible for data acquisition, method implementation, result validation, manuscript writing and manuscript proofreading; JQ.Z is responsible for data collection, experimental method design, results validation, financial support and manuscript proofreading; F.H is responsible for financial support and manuscript proof reading; X.L is responsible for data acquisition, result validation and manuscript proofreading; T.W is responsible for manuscript proofreading; All authors reviewed the manuscript. and have approved the submitted version.

Funding

We gratefully thank all the researchers who helped with this paper and also acknowledge the financial support from the National Natural Science Foundation Projects(52025093, 51979284) and Inner Mongolia Autonomous Region Water Conservancy Science and Technology Project (NSK202406).

Declarations

Competing interests

The authors declare no competing interests.

Ethics approval

The authors declare that this manuscript is original and has not been published previously in any other journal.

Additional information

Supplementary Information The online version contains supplementary material available at <https://doi.org/10.1038/s41598-025-29774-w>.

Correspondence and requests for materials should be addressed to J.Z.

Reprints and permissions information is available at www.nature.com/reprints.

Publisher's note Springer Nature remains neutral with regard to jurisdictional claims in published maps and institutional affiliations.

Open Access This article is licensed under a Creative Commons Attribution-NonCommercial-NoDerivatives 4.0 International License, which permits any non-commercial use, sharing, distribution and reproduction in any medium or format, as long as you give appropriate credit to the original author(s) and the source, provide a link to the Creative Commons licence, and indicate if you modified the licensed material. You do not have permission under this licence to share adapted material derived from this article or parts of it. The images or other third party material in this article are included in the article's Creative Commons licence, unless indicated otherwise in a credit line to the material. If material is not included in the article's Creative Commons licence and your intended use is not permitted by statutory regulation or exceeds the permitted use, you will need to obtain permission directly from the copyright holder. To view a copy of this licence, visit <http://creativecommons.org/licenses/by-nc-nd/4.0/>.

© The Author(s) 2025